TITLE:

A shift from pleiotropic to modular adaptation revealed by a high-resolution two-step adaptive walk

AUTHORS:

Grant Kinsler[1,2], Yuping Li[3,4], Gavin Sherlock*[,3], Dmitri A. Petrov*[,1]

AFFILIATIONS:

[1]Department of Biology, Stanford University
[2]Department of Bioengineering, University of Pennsylvania
[3]Department of Genetics, Stanford University
[4]Department of Microbiology & Immunology, UC San Francisco
*Equal contribution

ABSTRACT:

Evolution by natural selection is expected to be a slow and gradual process. In particular, the mutations that drive evolution are predicted to be small and modular, incrementally improving a small number of traits. However, adaptive mutations identified early in microbial evolution experiments, cancer, and other systems often provide substantial fitness gains and pleiotropically improve multiple traits at once. We asked whether such pleiotropically adaptive mutations are common throughout adaptation or are instead a rare feature of early steps in evolution that tend to target key signaling pathways. To do so, we conducted barcoded second-step evolution experiments initiated from five first-step mutations identified from a prior yeast evolution experiment. We then isolated hundreds of second-step mutations from these evolution experiments, measured their fitness and performance in several growth phases, and conducted whole-genome sequencing of the second-step clones. Here, we found that while the vast majority of mutants isolated from the first-step of evolution in this condition show patterns of pleiotropic adaptation - improving both performance in fermentation and respiration growth phases - second-step mutations show a shift towards modular adaptation, mostly improving respiration performance and only rarely improving fermentation performance. We also identified a shift in the molecular basis of adaptation from genes in cellular signaling pathways towards genes involved in respiration and mitochondrial function. Our results suggest that the genes in cellular signaling pathways are particularly capable of providing large, adaptively pleiotropic benefits to the organism due to their ability to coherently affect many phenotypes at once. As such, these genes may serve as the source of pleiotropic adaptation in the early stages of evolution, and once these become exhausted, organisms then adapt more gradually, acquiring smaller, more modular mutations.

INTRODUCTION

As organisms adapt to their environment, they face a multi-dimensional optimization problem. To be advantageous, new mutations must improve one or more traits under selection without imposing strong costs on other traits. Theoretical analyses of adaptive walks in multi-dimensional trait spaces suggest that mutations that generate small phenotypic shifts in few traits are more likely to be beneficial overall than mutations of large phenotypic effect on many traits (Orr 2000). Consequently, adaptive mutations are expected to both provide small fitness benefits and to be **modular** – that is, affect only a few traits without affecting others.

Despite these theoretical expectations, microbial evolution experiments have revealed that early adaptation often proceeds by single mutations that provide large fitness benefits (Y. Li, Petrov, and Sherlock 2019; Wiser, Ribeck, and Lenski 2013; Levy et al. 2015; Johnson et al. 2021; Venkataram et al. 2016). Moreover, in the cases where the improvement of these mutations has been decomposed into distinct trait performances, it is often observed that these mutations improve multiple traits simultaneously (as illustrated in Figure 1A) (Y. Li, Petrov, and Sherlock 2019; Y. Li et al. 2018; Bono et al. 2017; Jasmin and Kassen 2007).

The observation of adaptive mutations improving multiple performances at once, which we here term "**pleiotropic adaptation**", can be easily seen in a series of evolution experiments conducted with barcoded yeast in which a comprehensive set of adaptive mutations was profiled for their effects on likely orthogonal trait performances (Levy et al. 2015; Venkataram et al. 2016; Y. Li, Petrov, and Sherlock 2019; Y. Li et al. 2018). Li et al (2018) in particular showed that ~85% of first-step adaptive mutations isolated from their evolution experiment improve performance in both fermentation and respiration growth phases, both of which are under selection during the yeast growth cycle. These pleiotropic mutants from this initial step of adaptation, many of which harbor only a single mutation in the Ras/PKA pathway, are also strongly adaptive, providing fitness benefits of up to 120% per growth cycle (roughly 15% per generation) (Venkataram et al. 2016). Such large-effect Ras/PKA pathway mutations are commonly found in early evolution in other systems, such as cancer progression (Bailey et al. 2018). As the study we present here follows on from our previous series of findings, we use these yeast mutations as a motivating example throughout the rest of the introduction.

How do we reconcile our observations of pleiotropic adaptation (Y. Li et al. 2018) with theoretical expectations that these mutations should affect only a small number of traits? One possibility is that fermentation and respiration performances are not as distinct as we believe. However, a number of adaptive mutations do improve only one of these performances, demonstrating that it is in fact possible to shift one performance without affecting the other.

The other possibility is that the Ras/PKA pathway is wired in such a way that mutations that target this pathway are capable of being both pleiotropic and adaptive, affecting many phenotypes of the organism but in a coherent and coordinated fashion. It might be that

mutations in general might not have these patterns of pleiotropic adaptation and instead exhibit "**modular adaptation**", improving only a subset of the traits under selection. Thus, isolating and characterizing the effects of subsequent mutations, which may be less likely to target this already-mutated pathway, might better reflect the pleiotropic properties of adaptive mutations beyond these extremely beneficial first-step mutations in the Ras/PKA pathway. One way in which we can assess whether the observed adaptive pleiotropy is a common feature of adaptive mutations is to conduct adaptive walks, evolving populations further in the same environment. We can then ask whether later adaptive mutations continue to show pleiotropic adaptation or not.

One possibility is that pleiotropic adaptation is indeed common. This may be true if there are many pathways in the cell that can be mutated to yield simultaneous improvement of the traits under selection or, instead, if the signaling pathways mutated early can continue to be optimized beyond the first adaptive step. In this scenario, second-step adaptive mutations would continue to improve both traits under selection (Figure 1B, red points) and longer adaptive walks would also continue to show this pattern of pleiotropic adaptation (Figure 1B arrows).

Alternatively, pleiotropic adaptation may be rare, and first-step mutations target the only (or one of few) signaling pathway(s) which can result in simultaneous improvement of multiple traits (performance in both fermentation and respiration growth phases in the case of the yeast evolution experiments). For adaptation to continue, it would need to engage the modules that can independently control the performance in each growth phase. Individual second-step mutations under this scenario would then be expected to exhibit a pattern of "modular adaptation", improving only one performance under selection or the other (Figure 1C). The longer adaptive walks could continue down this route of specialization in either a single performance (blue or magenta arrows) or instead improve both performances under selection, but via sequential improvement of one performance and then the other (orange arrows).

Thus, to characterize the nature of single-step adaptive mutations and whether the observation of pleiotropic adaptation of first-step mutations is a general feature of individual adaptation-driving mutations or instead a rare feature of early adaptive mutations, we need to experimentally conduct high-resolution adaptive walks, wherein we can isolate adaptive mutations, quantify their effects on traits relevant to fitness, and identify the molecular basis of adaptation. The yeast barcoding system developed by (Levy et al. 2015) is particularly well-suited for this set of experiments, as we can isolate hundreds of mutations per evolution experiment and study their properties via pooled fitness measurement experiments.

In this study, we perform second-step evolution experiments using a set of five first-step adaptive mutations isolated from a glucose-limited evolution experiment (Levy et al. 2015) as new ancestors. We then isolate hundreds of mutants from these evolution experiments and measure their performance in the growth phases that make up the evolution condition. We find a shift in the nature of adaptation over this two-step adaptive walk. While first-step mutations

primarily demonstrate pleiotropic adaptation, improving performance in both growth phases under selection, second-step mutations instead primarily exhibit modular adaptation, improving performance in only a single growth phase under selection (Figure 1C). Whole genome sequencing reveals an associated shift in the molecular basis of adaptation: from first-step mutations in general signaling pathways to second-step mutations in genes related to mitochondrial function and respiration. Finally, we sample rare adaptive clones that showed patterns of adaptive pleiotropy and discovered that they harbor multiple additional mutations. This suggests that these populations have not yet reached physiological constraints but rather that adaptive walks may be constrained by genetic modules which prevent adaptive mutations from improving multiple performances in a single step.

This shows that early adaptation, here represented by the first-step in our evolution experiment, can engage signaling pathways that allow for rapid, large step pleiotropic adaptation but later adaptation is more likely to be modular, as expected by theory. We thus expect that longer term evolution will indeed progress through smaller, and ultimately more modular, adaptive mutations.

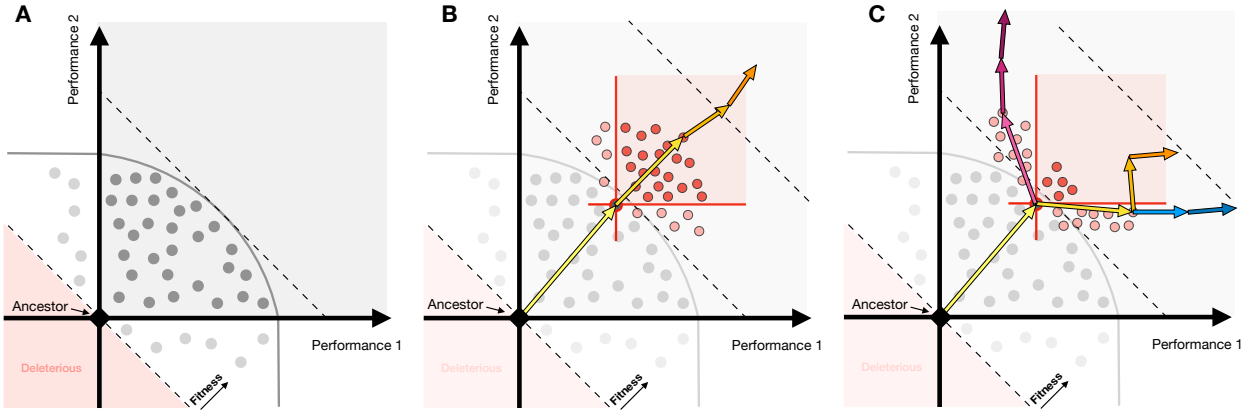

Figure 1. Theoretical illustration: Pleiotropy may be a generic feature of adaptation or specific to the first-step of evolution. (A) First-step adaptive mutations (each mutation depicted as a dot) in evolution often exhibit patterns of pleiotropic adaptation - improving performance in multiple traits simultaneously (falling into the gray square). Gray curved line represents the limits of combinations of performances reached by the first-step of evolution. **(B)** If pleiotropic adaptation is common, then second-step adaptive mutations (depicted in red) would continue to improve multiple performances at once. Longer adaptive walks would also continue to show these patterns (orange arrows). **(C)** If pleiotropic adaptation is rare and largely constrained to the first adaptive step, then second-step adaptive mutations might show a shift in their improvement, instead primarily improving one performance or the other (light red circles). In this scenario, longer term adaptive walks may continue to specialize in one performance or the other (depicted by blue and magenta arrows), or instead continue to collectively improve both performances, albeit in a stepwise manner (orange arrows).

RESULTS

Isolating second-step adaptive clones and measuring performance in growth phases

When yeast are grown in an environment under glucose-limitation in batch culture, they experience several growth phases (Figure 2A). First, the yeast experience lag phase, where they acclimate to the environment and allocate cellular resources to consuming glucose. Then, the yeast ferment the glucose, converting it to ethanol. Once the glucose is consumed, the yeast then undergo the diauxic shift and respire on the ethanol they produced during fermentation. Finally, once the supply of ethanol has been depleted, the yeast experience stationary phase, where they allocate resources to surviving without a carbon source. These growth phases are typically thought of as independent processes, with distinct transcriptional, proteomic, and metabolomic profiles that characterize and drive yeast physiology (DeRisi, Iyer, and Brown 1997; Schlossarek et al. 2022; Zampar et al. 2013; Murphy et al. 2015).

Previously, a population of barcoded yeast was evolved in a 2-Day transfer environment under glucose limitation, where they experienced lag, fermentation, and respiration but not stationary phases before being transferred to fresh medium (Levy et al. 2015; Venkataram et al. 2016). Adaptive mutations isolated from this experiment gained substantial fitness benefits, primarily by constitutively activating one of two glucose-sensing pathways: Ras/PKA and TOR/Sch9 (Venkataram et al. 2016). Additionally, 85% of these mutants improved performance in both fermentation and respiration phases, despite the supposed independence of these growth phases. Interestingly, with additional evolution experiments designed to maximize individual performances, Li et al (2019) were able to find evidence of constraints on the first step of evolution such that no single mutation is able to simultaneously maximize both fermentation and respiration performances to the largest extreme of each performance observed individually.

To understand whether pleiotropic adaptation is common or if instead first-step mutations represent rare solutions that improve both traits under selection, we carried out second-step evolution experiments in the same 2-Day transfer environment, isolated adaptive mutants, identified causative mutations underlying adaptation, and characterized the mutations' effects on performance in the environment's growth phases. Aggeli et al. (Aggeli, Li, and Sherlock 2021) previously performed second-step evolution experiments using barcoded populations that carried one of three mutations identified in the first step of evolution: a gain-of-function mutation in *CYR1*, a loss-of-function mutation in *GPB2*, and a gain-of-function mutation in *TOR1*. Here, we used additional barcoded populations derived from two distinct mutations in *IRA1*: one missense mutation and one nonsense mutation (see Methods). We then evolved 2 replicates of each barcoded population in the 2-Day transfer condition, labeled here "Evo2D", for 22 transfers (~176 generations) and isolated adaptive clones (Figure 2B,C). As we were also interested in how the number of traits under selection alters the extent of pleiotropic adaptation, we also evolved the same barcoded populations in a 3-Day transfer condition, herein termed "Evo3D", where populations experienced an additional 12 hours of respiration and 12 hours of stationary

phase, and isolated adaptive clones from this additional set of evolution experiments (Figure 2A-C; see Methods).

To assess the extent to which physiological and genetic constraints affect the second-step of adaptation, we quantified each mutant's performance in fermentation, respiration, and stationary growth phases using pooled barcoded fitness assays, as developed previously (Figure 2B; (Venkataram et al. 2016; Y. Li et al. 2018; Y. Li, Petrov, and Sherlock 2019; Kinsler, Geiler-Samerotte, and Petrov 2020; Kinsler et al. 2023). Briefly, we pooled all isolated second-step mutants together with the barcoded mutants from the first step of evolution. We then mixed this pool of barcoded yeast with a set of barcoded neutral lineages and the ancestral strain, such that the barcoded pool started at either 2% or 5% frequency in the population and the neutral barcoded lineages collectively represented 2% of the population (see Methods). We then measured the fitness of each mutant by serially transferring ~5x10^7 cells for five cycles in 1-, 2-, 3-, and 5-Day transfer intervals. At each transfer, we froze down the remaining cells, extracted their DNA, amplified the barcode region with PCR, and then sequenced the barcode region. We then calculated each mutant's fitness relative to the ancestor by comparing each mutant's frequency change with the pool of neutral lineages (Figure 2B, see Methods).

During the analysis of fitness measurement data, we observed that the detected fitness effects of each mutant varied systematically over the course of serial transfers during the fitness measurement of the isolated adaptive clones. Specifically, in the 2-Day transfer condition, many adaptive mutants showed very high fitness when the ancestral strain was at or above 80% of the population but showed much lower fitness at later time intervals when the pool of adaptive lineages dominated the population. We note that this effect is not due to change in population mean fitness, as this is already accounted for in these fitness values. While intriguing, we avoided these frequency dependent fitness effects in our data by using only early timepoints, where the ancestor dominated the population, as these reflect the fitness in the environment set by the ancestor and where the fitness of mutants isolated from the original evolution experiment matched their fitness measurements in previous experiments (Figure S1).

Second-step adaptive mutations provide substantial yet smaller fitness benefits than first-step mutations

We sequenced the barcodes in these populations to monitor the dynamics of evolution and to quantify the distribution of fitness effects. Using the approach implemented in software FitMut1 (Levy et al. 2015; F. Li, Tarkington, and Sherlock 2023), we quantified the distribution of fitness effects for these populations and the original evolution experiment. Because auto-diploidization is a common mode of adaptation in evolution experiments with haploid yeast, we also used a benomyl assay to determine the ploidy of the isolated adaptive clones (Figure 2C). We then categorized mutants according to their ploidy status and fitness across pooled fitness measurement experiments as neutral haploids, pure diploids, adaptive haploids, or high-fitness diploids (diploids that have additional beneficial mutations, see Methods).

We found that the rate of beneficial mutations is reduced in the second-step of evolution in the 2-Day environment, with adaptive mutations that provide fitness benefits of 1.0 or greater (per cycle) becoming much rarer (Figure 2D). This is consistent with the patterns of diminishing returns epistasis commonly observed in microbial evolution experiments (Wiser, Ribeck, and Lenski 2013; Johnson et al. 2021; Aggeli, Li, and Sherlock 2021; Good and Desai 2015; Wünsche et al. 2017; Chou et al. 2011; Kryazhimskiy et al. 2014). While we see this general decrease in the magnitude of the fitness benefit of adaptive mutations, we nonetheless find that many second-step adaptive mutations still have substantial fitness gains in the 2-Day transfer evolution condition. Across all isolated second-step adaptive mutants (excluding auto-diploids and neutral haploids), the average fitness benefit provided is 82% per cycle relative to the parental strain. This is similar across mutants isolated from both 2- and 3-Day evolution experiments (Figure 2E,F). We also sampled rare mutants with fitness advantages as high as or even higher than the most extreme fitnesses observed in the first step of evolution. For example, two mutants isolated from the Evo3D *IRA1-missense* evolution experiments provide a benefit of ~200% above the parental *IRA1-missense* strain, which corresponds to a ~350% fitness advantage per 2-Day cycle over the original ancestor strain (Figure 2E,F). As will be discussed later, these extremely fit mutants represent rare and complex mutations, sometimes consisting of up to four distinct adaptive mutations.

We also calculated the relative fitness improvement provided by auto-diploidization alone by comparing the fitness of the pure diploid population to the neutral haploids for each parental strain. Consistent with the pattern of diminishing epistasis observed from the evolution trajectories, we find that the fitness benefit of auto-diploidization has decreased in the second step of evolution from 95% per cycle in the first-step of evolution to 63% on average across all second-step auto-diploids (Figure 2F). However, this number varied by parental strain, with *TOR1* auto-diploids providing the largest fitness benefit of 81% per cycle and auto-diploids of Ras/PKA parental strains providing fitness benefits of 55%, 48%, and 52% per cycle to *CYR1, GPB2, and IRA1-missense*, respectively (Figure 2F). Surprisingly, we did not isolate any auto-diploids from the *IRA1-nonsense* evolution experiments. We suspect this could be due to differences in the fitness benefit provided by auto-diploidization to *IRA1-nonsense* strains compared to other beneficial mutations in the same evolving population or reduced auto-diploidization rate in this genetic background.

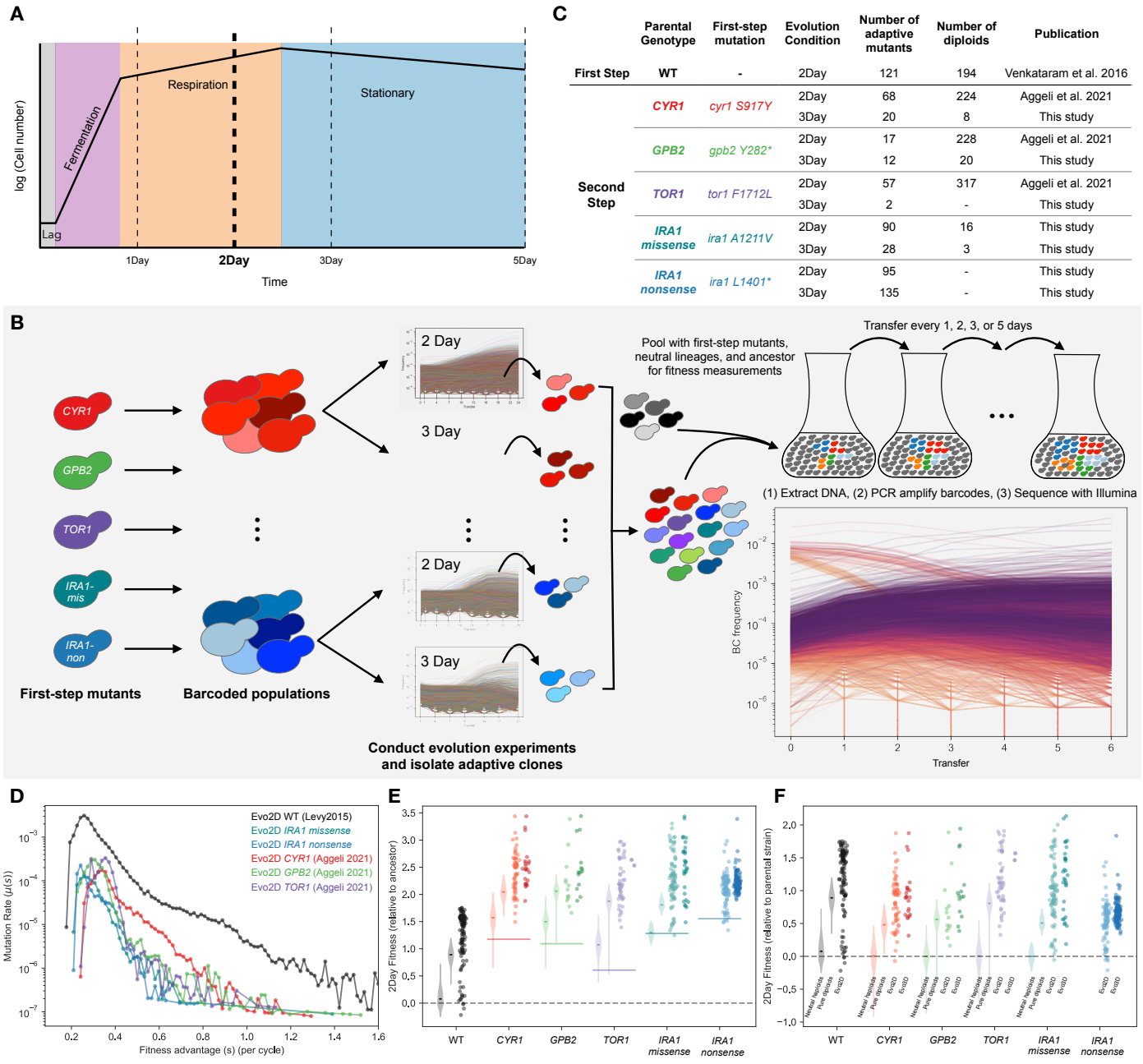

C

	Parental Genotype	First-step mutation	Evolution Condition	Number of adaptive mutants	Number of diploids	Publication
First Step	WT	-	2Day	121	194	Venkataram et al. 2016
Second Step	*CYR1*	*cyr1 S917Y*	2Day	68	224	Aggeli et al. 2021
			3Day	20	8	This study
	GPB2	*gpb2 Y282**	2Day	17	228	Aggeli et al. 2021
			3Day	12	20	This study
	TOR1	*tor1 F1712L*	2Day	57	317	Aggeli et al. 2021
			3Day	2	-	This study
	IRA1 missense	*ira1 A1211V*	2Day	90	16	This study
			3Day	28	3	This study
	IRA1 nonsense	*ira1 L1401**	2Day	95	-	This study
			3Day	135	-	This study

Figure 2. Summary of experiments and fitness effects of isolated adaptive mutants. (A) A schematic of yeast growth phases under the nutrient conditions used in this study. The yeast experience 4 hours of lag phase, 16 hours of fermentation and 4 hours of respiration phase in the first 24 hours of growth. **(B)** Schematic of barcoded evolution experiments and fitness measurement experiments. **(C)** Table of mutants used in this study, including ploidy, and publication source.**(D)** Probability density of mutational fitness coefficients. The black line refers to first-step mutants from Levy et al 2015. Colored lines depict the inferred density of fitness effects of mutations from second-step evolution experiments in the 2Day transfer environment (Evo2D). **(E)** Fitness effects per cycle in 2-Day transfer of all mutants, relative to WT ancestor. First violin plot for each parental strain shows neutral haploids. Second shows pure diploids. Third column is all other 2-Day adaptive mutants, including adaptive haploids and high-fitness diploids. Fourth column is all other 3-Day adaptive mutants. **(F)** As in (E), but relative to parental strain.

Second-step adaptive clones demonstrate a shift from pleiotropic to modular adaptation

Next, to determine whether the pattern of pleiotropic adaptation observed over the first-step of evolution is maintained in the second step, we compared changes in performance for each mutant to its parental strain. To calculate each mutant's performance in fermentation, respiration, and stationary phases, we leveraged differences in each mutant's fitness in experiments of different transfer lengths, which was previously shown to be a good proxy for the direct performance in each growth phase (Y. Li et al. 2018; Y. Li, Petrov, and Sherlock 2019). In particular, a mutant's respiration performance per hour was calculated as the difference between its 2-Day fitness and 1-Day fitness, divided by the 24 hours in respiration phase experienced over the second day (Figure 3A). We then used this respiration performance to extrapolate the mutant's relative fitness at 20 hours, the time at which the population undergoes the diauxic shift from fermentation metabolism to respiration metabolism, with which we can calculate its fermentation performance per hour (Figure 3A). Finally, we calculated a mutant's stationary performance by taking the difference between 5- and 3-Day fitness and dividing it by the 48 hours of stationary phase experienced over these two days (Figure 3A). Importantly, the growth phase performances calculated here reflect compound measurements of several parameters important to fitness during and between growth phases, including energy metabolism, sensing of changing nutrient gradients, and survival.

We found that while 85% (±3%) of isolated first-step adaptive mutants improved performance in both fermentation and respiration phases (black points within gray square in Figure 3B), only 35% (±1%) ($p<0.001$, re-sampling test) of isolated second step adaptive haploids evolved in the same 2-Day transfer environment improved performance over their first-step parental strain in both phases (light orange points within gray square in Figure 3B). Second-step mutants that were isolated from Evo3D, which encompasses the growth phases of Evo2D, show an even stronger shift from adaptive pleiotropy than the second-step mutants from the Evo2D, with only 13% (±1%) of these mutants improving performances in both fermentation and respiration (darker colored points labeled "Evo3D" in Figure 3B, C). This shift is also seen for each parental strain individually (Figure 3C), with Evo2D second-step mutants isolated from each first-step parental strain showing a reduction in the number of mutations that improve performance in both fermentation and respiration, albeit with some variability in magnitude. For example, only 25% (±2%) and 17% (±2%) of second-step Evo2D mutants from *IRA1-missense* and *IRA1-nonsense* parental strains, respectively, improved both fermentation and respiration performances (Figure 3C). At the same time 51% (±4%), 65% (±10%), and 65% (±5%) of second-step Evo2D mutations improve both fermentation and respiration performances from *CYR1*, *GPB2*, and *TOR1*. Thus while the second step adaptive mutations are still capable of improving fermentation and respiration performances at the same time, the probability of mutations being pleiotropically adaptive is lower.

In addition to a reduction in the number of second-step mutations that improve performance in both fermentation and respiration phases, we noticed that second-step mutants were much

more likely to improve respiration performance than fermentation performance. Across all second-step Evo2D mutants, 98% (±1%) improved respiration performance. 61% (±1%) of these mutants improved respiration at the cost to fermentation performance (Figure 3B). This effect is even stronger for Evo3D mutants, where 86% (±1%) improve respiration at a cost to fermentation performance (Figure 3B). This trend holds across most parental strains, with the strongest pattern seen for mutants evolved from the *IRA1-nonsense* parental strain, where 81% (±2%) of Evo2D mutants and 96% (±2%) of Evo3D mutants improved respiration performance at the cost of fermentation performance. Note that while many of these mutants reduce fermentation performance from the initial first-step parental strains, only a small number of mutants have fermentation performances worse than the original ancestor strain (Figure 3C, vertical black dashed line in each subplot).

At the same time, improving performance in only the fermentation phase is rare. Only 2% of second-step Evo2D mutants and no isolated second-step Evo3D mutants improve fermentation alone, despite the fact that an equivalent improvement in fermentation performance would result in similarly high fitnesses for those mutants in the 2-Day condition these populations were evolved in (see fitness isoclines in Figure 3C).

Despite these general patterns revealing a shift from pleiotropic to modular adaptation, there are several examples of very strongly adaptive clones which improve both performances. For example, one clone isolated from the *IRA1*-missense population has a fitness advantage of 340% per cycle relative to the initial ancestor (or 210% relative to the *IRA1*-missense parental strain). This mutant does improve performance in both fermentation and respiration growth phases, albeit with most of its fitness gain coming from respiration (Figure 3C, *IRA1*-missense panel, labeled with red arrow). We isolated other rare examples of very fit clones that improve both growth phases from other parental strains (Figure 3C, *IRA1*-nonsense panel, labeled with red arrows), suggesting that the yeast have not yet reached functional constraints on the ability to improve both fermentation and respiration performance and that it is still possible to improve both performances beyond the evolutionary constraints observed for the first step of adaptation. As discussed below, some of these very fit clones have acquired third or fourth adaptive steps, allowing them to achieve these high fitnesses.

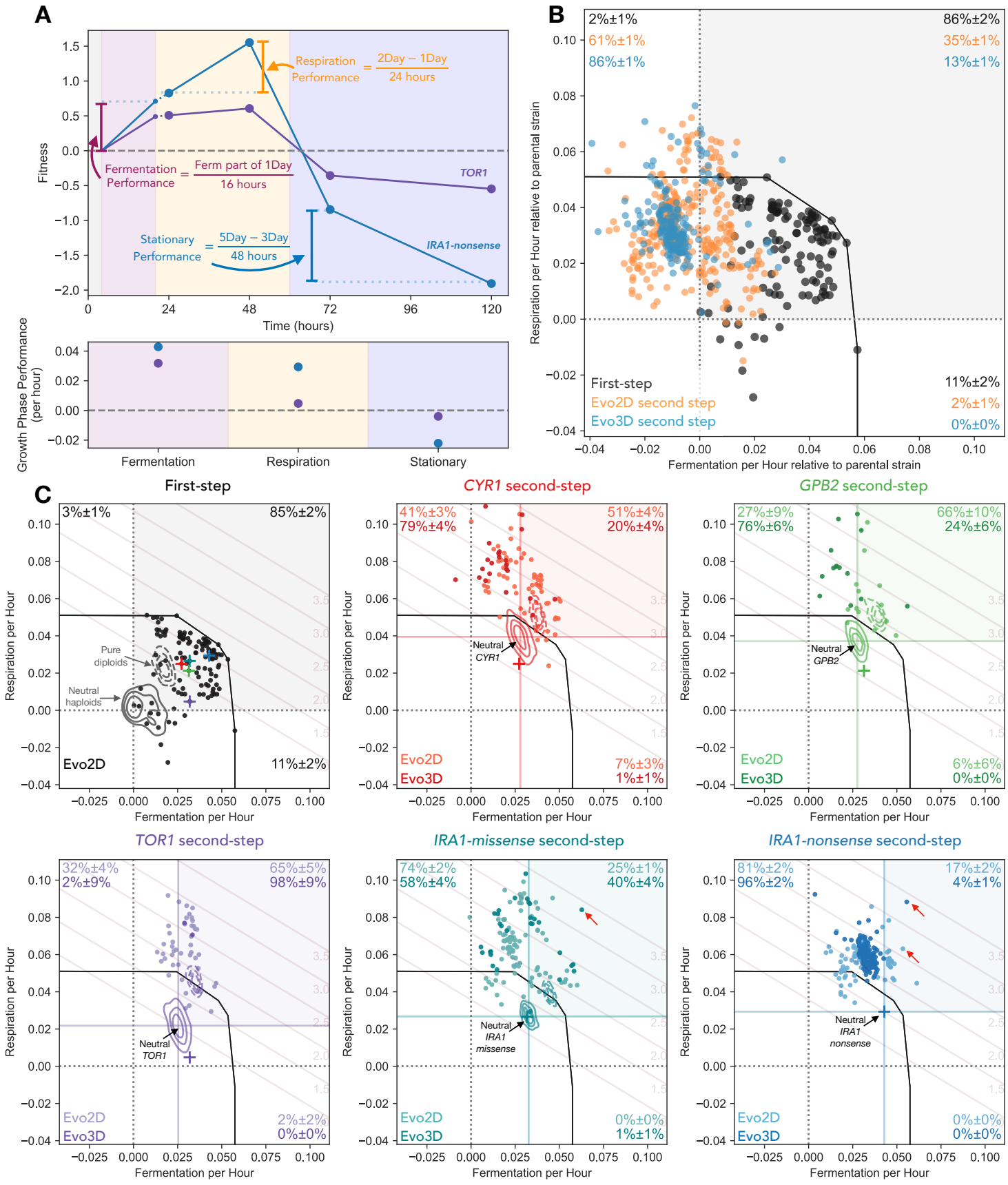

Figure 3. Second-step adaptive mutants tend to improve respiration performance and not fermentation performance. (A) Performance calculation in each growth phase. Respiration performance (per hour) is calculated as the difference between a mutant's 2-Day and 1-Day fitness, divided by 24 hours. To calculate fermentation performance (per hour), we remove four hours of 1-Day fitness that is due to the mutant's respiration benefit. The remaining fitness is then divided by 16 hours of fermentation phase. Stationary phase performance (per hour) is calculated as the difference between 5- and 3-Day fitness divided by 48 hours. Example fitnesses and performances are shown for the *TOR1* and *IRA1-nonsense* mutations used as parental strains for the second-step of evolution. **(B)** Comparison of changes in performances from first- to second-step mutants relative to each parental strain. Note that first-step mutants are shown relative to the initial ancestor (the same as their measured fitness). Second-step mutants are shown relative to the relevant parental strain (i.e. second-step mutants from *IRA1-*missense are shown relative to neutral *IRA1-missense* parental lineages). Percentages in corners indicate estimated fraction of mutants in each quadrant as determined by re-sampling of mutants with fitness measurement error. **(C)** Performance of isolated mutants separated by parental strain**.** Each mutant's performance in fermentation and respiration growth phases is shown, separated into subfigures by the initial ancestor for each mutant. KDE estimates represent the density of neutral haploids (solid lines) and pure diploids (dashed lines) for each ancestor. Crosses represent the barcoded mutants carrying the first-step mutation from the initial evolution experiment. Black line depicts a convex hull of the most extreme first-step mutants. Fitness isoclines show the 2-Day fitness advantage per cycle relative to ancestral strain associated with each location in the performance space.

Adaptively modular second-step mutants are more likely to improve performance in stationary phase

We next asked how the shift from adaptive pleiotropy to adaptive modularity of performances under selection affects how these mutants perform in other tasks not under selection in the Evo2D environment. For example, Li et al (2018) (Y. Li et al. 2018) showed that many of the first-step mutations, which tended to improve both fermentation and respiration performances, exhibited costs in stationary phase performance. Does the shift towards adaptive modularity reduce the likelihood or magnitude of costs in other performances, potentially indicating that these mutants are more modular overall? Or do these costs to other performances remain?

To address these questions, we calculated each mutant's performance in stationary phase (Figure 2A). As previously described (Y. Li et al. 2018), first-step mutants are more likely to incur a cost in stationary phase than to improve it (Figure 4A), with 30% (36/119) of mutants showing such a cost (Figure 4B) and less than 2% (2/119) showing any improvement in stationary performance. The most fit first-step mutants which improve both fermentation and respiration performance to substantial degrees tend to have larger costs in the stationary phase. In particular, the *IRA1*-nonsense mutants, which were the most fit in the first-step, have the strongest costs in stationary phase performance, up to -4% per hour (Figure 4A).

We find that many Evo2D second-step mutants do pay a cost in stationary phase. In particular, 42% of second-step Evo2D adaptive mutants have lower stationary performance than their parental strain. At the same time, these costs to stationary performance tend to be somewhat

minor, exhibiting costs of less than -2% per hour for second-step mutants derived from *CYR1*, *GPB2*, *TOR1*, or *IRA1*-missense parental strains (Figure 4B). Note that this was not the case for the second-step mutants isolated from *IRA1*-nonsense populations, which exhibited the strongest costs to stationary phase in the first-step of evolution. These second-step mutants had further costs to stationary performance as extreme as -10% per hour (see supplemental figures S3 and S4).

However, in contrast to the first-step of evolution where stationary performance was rarely improved, 25% (77/306) of second-step Evo2D mutants show an increase in stationary performance (Figure 4A). We further stratified the second-step mutants based on their combined fermentation and respiration performances. Specifically, we asked whether mutants that only improve respiration performance showed behavior in stationary phase that was distinct from those that improved both fermentation and respiration performance. We find that second-step Evo2D mutants that only improved respiration performance had varied effects on stationary performance, with 36% (70/197) showing increased stationary performance and 39% (76/197) showing a cost to stationary performance. By contrast, second-step Evo2D mutants that improved both fermentation and respiration performances were much less likely to improve stationary performance, with only 6% (7/109; $p<1e-8$ compared to by respiration-only improvers by Fisher's exact test) of these mutants showing stationary improvement and 49% (53/109) imposing a cost on yeast's ability to survive stationary phase.

Thus, it appears that mutations that are capable of improving both fermentation and respiration at the same time are more likely to incur costs in stationary phase. This inherent relationship may explain the reduction in Evo3D mutants that improve both fermentation and respiration performances (Figure 3B, 4A), as stationary phase is additionally under selection in this condition. Indeed, 79% (160/202; $p<1e-8$ compared to Evo2D by Fisher's exact test) of Evo3D mutants show an improvement in stationary phase, 97% (155/160) of which do not improve fermentation. While 7% (15/202) of Evo3D mutants do exhibit a cost in stationary phase, these costs are relatively minor and are primarily found in mutants with combined fermentation and respiration performances that compensate for these costs to stationary performance (Figure 4A and B). These data indicate that the shift from mutants that improve both fermentation and respiration performances to those that primarily improve respiration performance is accompanied by a change in stationary phase performance. This pattern is true even when the other performance (stationary phase) is not under selection, as is in the case of Evo2D, suggesting that the pleiotropic "side effects" - that is phenotypic effects of mutations that are not primarily under selection (Kinsler, Geiler-Samerotte, and Petrov 2020) - of these second-step mutants may differ more generally from those of the first-step mutants.

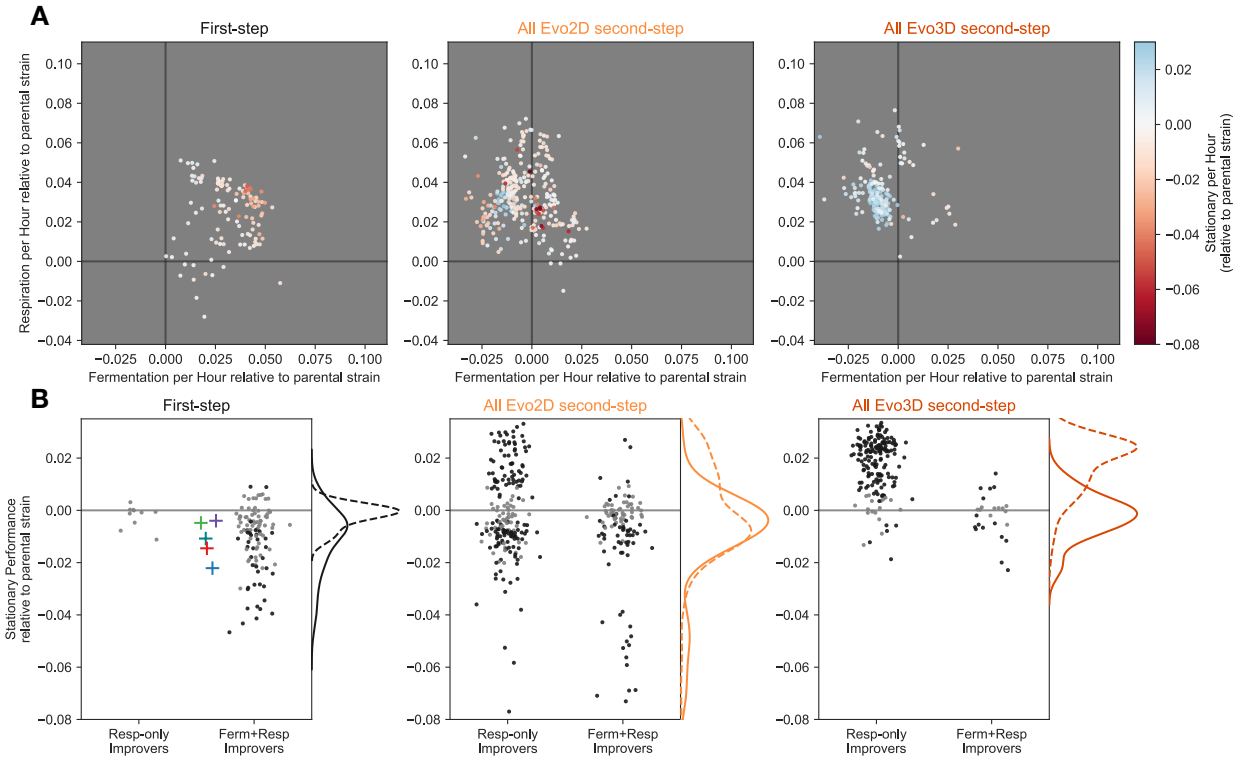

Figure 4. Mutations that improve respiration performance only exhibit less extreme costs in stationary phase compared to those that improve fermentation and respiration performances. (A) Each panel depicts mutant performance relative to their parental strain, colored by the relative stationary phase performance of the parental strain (see color bar). The first panel shows all first-step mutants. The second and third panels depict second-step mutants isolated from Evo2D and Evo3D conditions, respectively. **(B)** Each panel shows the stationary performance relative to the mutants' respective parental strains. Mutants are split according to the effect on fermentation and respiration performances. Those which improve both fermentation and respiration are categorized as "Ferm+Resp Improvers" and all other mutants are categorized as "Resp-only improvers". Black points represent those with measurement error that does not overlap 0. Gray points have measurement error that show no significant change in stationary performance relative to the parental strain. Panels are organized as in (A). Kernel density estimates show the relative density for respiration-only improvers (dashed line) and fermentation and respiration-improving mutants (solid line).

Changes in selection pressure and physiological limitations do not explain the shift towards modular adaptation

Thus far, we have shown that there is a general shift in the effect that adaptive mutations have on performance in growth phases over the course of a two-step adaptive walk. In particular, we find that while first-step mutations exhibit adaptive pleiotropy, improving both fermentation and respiration performances, second-step mutations isolated from the same Evo2D environment tend to be adaptively modular, improving only respiration performance and often at the cost to fermentation performance. What could be driving this shift? There are three primary possibilities for this observation. One possibility is that, while care was taken to ensure the evolution condition was as consistent as possible to the first step of evolution, the selection pressure in

the second-step evolution experiments was shifted to favor respiration performance more than fermentation performance. A second possibility is that the populations have reached physiological limits on the yeast's ability to ferment glucose, such that there is more room to improve respiration performance. Finally, it could be that genetic and signaling pathways are wired such that there are only a limited number of mutational targets available to further improve both fermentation and respiration performances in the second-step of evolution.

The first possible explanation for the shift towards modular adaptation is that the second-step of evolution was accompanied by a change in the relative contribution of fermentation and respiration growth phases to fitness in the 2-Day transfer condition. While we took care to ensure that the population sizes, transfer times, media conditions, and other details were identical to the conditions used in the first-step evolution experiment, it could be possible that differences remain. For example, the identity of the strain comprising the majority of the population in second-step evolution experiments may have shifted the selection pressures to increase the importance of respiration performance compared to the first step of evolution. To test whether there was such a shift, we compared the fitness effects of mutations in the evolution experiment itself with our fitness measurement experiments, which more closely mimic the first-step evolution experiments because the ancestral strain comprises the majority of the population. Specifically, we calculated the partial correlation between respiration performance and fitness during the evolution experiment, accounting for the fitness inferred from our fitness measurement experiments. If respiration performance contributes more to evolution fitness than expected from our fitness measurement experiments, we would expect a positive partial correlation after this adjustment. However, this is not the case ($r=-0.02$, $p=0.74$), indicating that the shift from pleiotropic to modular adaptation is not due to a change in selection pressure (see Methods, Differences in selection pressure do not drive shift towards modular adaptation).

The second possible explanation for the shift towards modular adaptation is that the yeast have reached physiological limits on the ability to improve fermentation performance. To test whether yeast have reached the upper limits of fermentation performance, we performed additional evolution experiments in a 1-Day transfer environment, which primarily selects for fermentation performance. From these experiments, we isolated at least one second-step mutation from the *IRA1*-nonsense population that improved fermentation performance above the highest fermentation performances achieved by first- or second-step mutations evolved in the 2-Day and 3-Day environments (see Fig S2). This suggests that while a fermentation performance maximum has not yet been reached, the pre-existing wiring of genetic and signaling pathways may be such that it is much easier to find mutations that improve respiration performance at the cost of fermentation performance than it is to find mutations that improve both fermentation and respiration performances or even fermentation performance at the cost to respiration performance.

Second step adaptive mutations reveal a shift from mutational targets in general nutrient-sensing pathways to specific processes involved in mitochondrial function

To better understand these patterns of pleiotropy and to identify the genetic basis of adaptation in these environments, we performed whole-genome sequencing on 324 adaptive mutants and called variants (see Methods). To identify the likely adaptive mutations, we compared the genes across all isolated mutants from all evolution experiments and labeled genes that were hit more than three times across all mutants as putatively causal. After identifying pathways that were recurrently targeted, we further identified genes belonging to the same pathways and called these as putatively causal as well.

From this whole-genome sequencing, we found some adaptive targets in nutrient-sensing pathways that were previously identified in the first-step of evolution. The first-step of adaptation typically involved mutations in one of two signaling pathways responsible for sensing glucose and instructing the cells to grow: the Ras/PKA and TOR/Sch9 pathway (Venkataram et al. 2016), Table 1). Most of these mutations resulted in loss of function in negative regulators of the pathway or modification of function in positive regulators, ultimately driving constitutive activation of these pathways (Venkataram et al. 2016). In an analysis of the second-step of evolution for *TOR1*, *CYR1*, and *GPB2* mutants in the 2-Day environment, Aggeli et al (2021) identified Ras/PKA pathway mutations as an adaptive route for *TOR1* mutants and TOR/Sch9 mutants as an adaptive route for *CYR1* and *GPB2* mutants. The additional sampling we've conducted here, including sequencing mutants isolated from the two *IRA1* populations under Evo2D and Evo3D, further confirm that TOR/Sch9 pathway mutations are commonly observed in the background of Ras/PKA mutants. In particular, we find that mutations in the gene *KSP1*, a PKA-activated kinase which inhibits autophagy via TORC1 (Umekawa and Klionsky 2012; Chang and Huh 2018), are common across all of the Ras/PKA parental strains (Table 1). These mutations were most commonly isolated from *IRA1*-nonsense populations, where 42% (32/77) of Evo2D mutants and 91% (30/33) of Evo3D mutants harbored a *KSP1* mutant. Unlike the TOR/Sch9 pathway mutants observed in the first-step of evolution, which putatively result in increased TORC1 activity, increased cell growth, and decreased autophagy (Wilson and Roach 2002; Venkataram et al. 2016), many of the observed second-step *KSP1* mutations are loss-of-function . This indicates that these mutations may be acting in the opposite direction of first-step mutations in this pathway, potentially allowing for the up-regulation of TOR despite (or in compensation of) increased activation of PKA associated with the Ras/PKA mutants.

Beyond mutations in nutrient-sensing signaling pathways commonly being observed in the first-step of adaptation, our sampling reveals a shift towards mutational targets related to mitochondrial function and respiration, which likely affect the respiration performance of mutants measured in our study (Table 1). In particular, we find that 36% (22/64) of adaptive mutants isolated from *IRA1*-missense populations in the 2-Day evolution condition acquire mutations in or near genes involved in the TCA cycle (*CIT1*, *KGD1*, *MDH1*, *MAE1*, *ALD5*). Interestingly, all of these mutations are either missense or putatively regulatory mutations in enzymes directly

responsible for respiration, suggesting they may modify the function or expression of these enzymes, potentially changing respiratory flux (Suissa, Suda, and Schatz 1984; Kurita and Nishida 1999; Navarro-Aviño et al. 1999; Repetto and Tzagoloff 1989; Ait-El-Mkadem et al. 2017; Reinders et al. 2007; McAlister-Henn and Thompson 1987; Boles Eckhard, de Jong-Gubbels Patricia, and Pronk Jack T. 1998). In addition, we identified mutations in several genes related to the regulation of respiration and mitochondrial function, with 25% (16/64) of isolated 2-Day *IRA1*-missense mutants identified as carrying a mutation in the RTG pathway, which is responsible for the regulation of genes important for respiration. In particular, we observe putative loss-of-function mutations in *MKS1*, a negative regulator of the RTG pathway, and missense mutations in *RTG2*, a positive regulator of the pathway (Liu et al. 2003; Liao and Butow 1993; Komeili et al. 2000; T. Sekito, Thornton, and Butow 2000; Takayuki Sekito et al. 2002). This suggests that these mutations may be up-regulating the RTG pathway and the genes it regulates, indirectly increasing metabolic flux through the TCA cycle. Moreover, 19% (12/64) of these mutants carry a mutation in other genes related to the regulation of mitochondrial biogenesis (*PUF3*, *PAB1*, *PAN1*, *PAN2*, *AIM17*), many of which are related to post-transcriptional modification of mRNA molecules related to mitochondrial function or respiration (Chaithanya and Sinha 2023; C.-D. Lee and Tu 2015; Lapointe et al. 2018).

These patterns are also observed in other populations harboring different first-step mutants. In particular, while our sampling for *IRA1-nonsense* and *IRA1-missense* populations allowed us to detect the largest number of mutational targets, mutations in genes involved in the TCA cycle, RTG pathway, and mitochondrial biogenesis were found in populations from nearly all first-step mutations, with a few exceptions. These exceptions, for example the absence of HOG-pathway mutations from *IRA1*-missense and *IRA1*-nonsense backgrounds, is suggestive of historical contingency, where the identity of further mutations is dependent on mutations acquired earlier in evolution (Blount, Borland, and Lenski 2008; Harms and Thornton 2014; Park, Metzger, and Thornton 2022; Bakerlee et al. 2021). While some of these genes were detected in previous work (Aggeli, Li, and Sherlock 2021), additional sampling from new evolution experiments in the 3-Day condition and additional parental strains (*IRA1*-missense and *IRA1*-nonsense) allowed us to more confidently identify recurrently mutated genes and to group the observed sets of mutations and genes into functional categories and pathways.

Mutations isolated from the 3-Day evolution experiment are a subset of 2-Day adaptive mutants

We next examined whether there was a difference in the mutational targets isolated from 2- and 3-Day evolution experiments, given that we observed that Evo2D mutants were more likely to improve both fermentation and respiration performances than Evo3D mutants (Figure 3), and Evo3D mutants were more likely to improve stationary performance than Evo2D (Figure 4). In particular, we wondered whether the addition of stationary phase as a selective pressure allowed for new mutational targets to be adaptive because of their effect on stationary phase, or

582 if instead, the addition of stationary phase restricted the Evo3D mutational targets to a subset of
583 the Evo2D mutations that were not costly to stationary performance.
584
585 By comparing the sets of mutated genes for well-sampled parental strains *IRA1-missense* and
586 *IRA1-nonsense*, we saw that all genes mutated in the 3-Day evolution experiments were also
587 identified in the 2-Day evolution experiments (see Table 1). In particular, *PUF3*, *PAB1*, and
588 *MTH1* mutants are entirely absent as single mutations from the 3-Day *IRA1*-nonsense
589 experiments, shifting the molecular targets to essentially just those in *KSP1*. Similarly, RTG and
590 TCA cycle mutants are reduced in frequency or absent from the 3-Day *IRA1*-missense
591 experiments, respectively. As expected, these mutations that are reduced in frequency show
592 costs in stationary performance and thus have reduced fitness in the 3-Day transfer
593 environment (Figs S7 and S8).

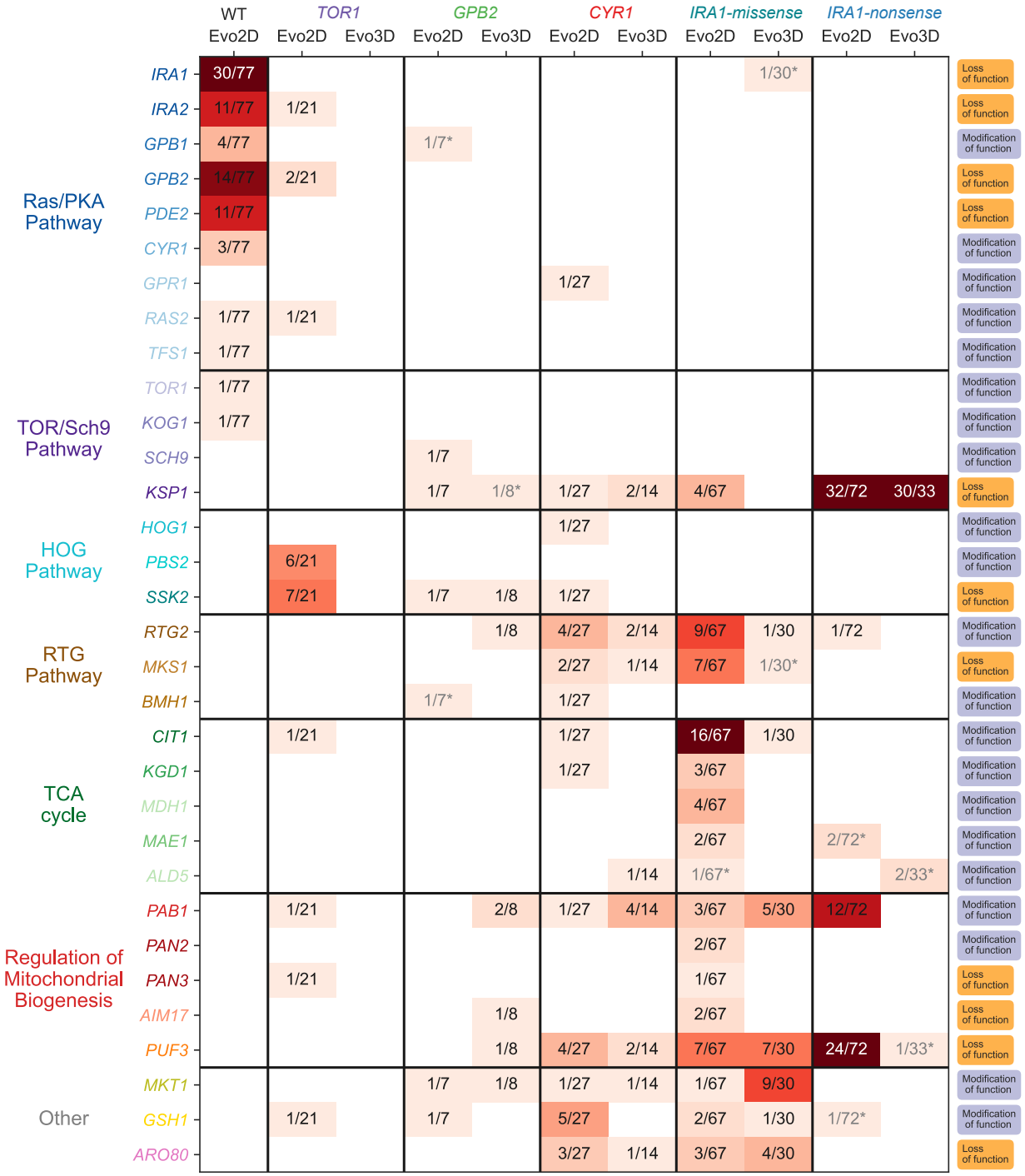

Table 1. Identified mutations by ancestral genotype and evolution condition. Boxes with gray text and asterisks indicate genes mutated only in the context of other putatively causal mutants. The column on the far right indicates the putative functional effect of the mutations on the gene. If any stop-gained or frameshift mutations were identified in this gene, it was classified as harboring "loss of function" mutations. If instead, only missense or nearby non-genic mutations were identified, the gene is classified as "modification of function".

The exhaustion of mutational targets in nutrient-sensing signaling pathways drives the shift towards modular adaptation

To understand how the shift from pleiotropic to modular adaptation over the two-step adaptive walk is reflected on a molecular basis, we examined how each of these mutations moved the organisms in the performance space. The first step of evolution, which primarily hit mutational targets in the Ras/PKA pathway, shows strong patterns of pleiotropic adaptation, with these mutations improving both fermentation and respiration performances (Figure 5A).

Of the second-step adaptive haploids, those with mutations in the Ras/PKA pathway (Figure 5B, blue circles), which were isolated primarily from the *TOR1* populations, also display pleiotropic adaptation, improving both fermentation and respiration performance. This suggests that mutations which putatively increase the activity of the Ras/PKA pathway are indeed generally adaptively pleiotropic.

In addition to Ras/PKA mutations, other haploids with mutations in *ARO80* (Figure 5B, pink circles) and *GSH1* (Figure 5B, gold circles), show recurrent patterns of pleiotropic adaptation across parental strains, notably across *CYR1* and *IRA1*-missense genetic backgrounds (Figures S5 and S6). Mutations in these genes, which are involved in amino acid catabolism (Iraqui et al. 1999; K. Lee and Hahn 2013) and glutathione biosynthesis (Kistler, Maier, and Eckardt-Schupp 1990), respectively, may be adaptively pleiotropic due to their involvement in processes entirely orthogonal to, or upstream of, both fermentation and respiration.

Many of the remaining mutational targets improve respiration performance at the cost of fermentation performance. In particular, haploid mutants which harbor mutations in genes involved in the TCA cycle (Figure 5B, green circles), mitochondrial biogenesis (orange, red circles), or the RTG pathway (brown circles) improve respiration performance at the cost to fermentation performance in *CYR1*, *GPB2*, *TOR1*, and *IRA1*-missense backgrounds when present (Figure 5). Notably, haploids that harbor mutations in these genes have similar fitness in the 2-Day transfer environment to mutants with mutations in *ARO80* and *GSH1*, which exhibit adaptive pleiotropy. Despite these similar fitnesses, there is an 8-fold increase in observed adaptively modular genetic targets than those that are adaptively pleiotropic in the *IRA1*-missense 2-Day evolution experiments (41 mutants in TCA and RTG with fitnesses between 2.0 and 2.5 compared to 5 in *GSH1* and *ARO80* for *IRA1*-missense).

There are also single point mutations in *MKT1* which achieve very high 2-Day fitness by greatly improving respiration performance and showing little cost to fermentation performance (Figure 5B - chartreuse circles). Interestingly, all adaptive mutations in this gene occur at the same nucleotide, changing from 89A to C,G, or T. Thus, while these mutations are driven by only a single mutation, their lower frequency reflects the reduced target size compared to the other haploid mutations which have multiple targets within the gene (e.g., those in RTG pathway, TCA cycle, etc.). The 89A allele is a derived allele in the parental S288C yeast strain used for all of

these experiments and reflects an ancestral reversion in the case of A89G. This A89G reversion has been previously observed in other evolution experiments in glucose limitation and the 89G allele has been shown to stabilize mRNA of mitochondrial genes that are targets of Puf3 (Chaithanya and Sinha 2023; Gupta et al. 2015). Interestingly, 89C and 89T alleles each provide similar fitness benefits as the 89G allele in our experiments despite resulting in distinct amino acids, suggesting that the 89A allele and the resulting aspartic acid may be particularly costly to *MKT1* function.

Beyond adaptive mutations in haploids, auto-diploidization is a common mode of adaptation. In particular, we see that in addition to diploidy being adaptively pleiotropic by itself (pure diploids shown as topographical Kernel Density Estimates in Figure 5), high-fitness diploids that co-occur with other mutations (colored triangles in Figure 5) also show patterns of adaptive pleiotropy, improving both fermentation and respiration performances. This seemingly universal benefit without cost likely explains the high frequency of auto-diploidization observed across genetic backgrounds and environmental conditions in many yeast evolution experiments (Tung et al. 2021; Venkataram et al. 2016; Levy et al. 2015; Hong and Gresham 2014; Fisher et al. 2018). While these high-fitness diploids provide a much larger benefit than haploids that harbor mutations in the same genes, their reduced frequency is likely due to a lower mutation rate, as these mutants needed to acquire both a mutation in an adaptive target and auto-diploidize, together improving respiration to a larger extent and mostly eliminating costs to fermentation performance associated with the mutation. Notably, most of the point mutations are homozygous, indicating they likely occurred before the auto-diploidization event.

In addition to these general trends, we sampled a small number of mutations that have a total of three or four putatively causal mutations since the original ancestor. These mutants provide hints about how adaptation might proceed over longer adaptive walks. In one case, as demonstrated by the *IRA1*-nonsense + *KSP1* + *PUF3* mutant depicted in the second panel of Figure 5C, we observe adaptation as continuing down a route towards specialization in respiration performance. We also observe three examples where the collective effect of the mutations instead drives evolution towards generalism – improving both fermentation and respiration performance – despite being composed of second-, third-, and fourth-step mutations which tend to improve only one performance or the other. For instance, one *IRA1*-missense mutant acquired an *IRA1*-nonsense mutation, an *MKT1* A89G mutation which improves only respiration by itself in this background, and acquired a mutation in *SPB1* (Suppressor of *PAB1*), which is expected to improve only fermentation with a modest cost to respiration, assuming additive mutational effects in the performance space (Figure 5C, first panel). We see similar examples for two *IRA1*-nonsense mutants: one of which acquired both *KSP1* and *GSH1* mutations and the other of which acquired *KSP1* and *TAN1* mutations (Figure 5C, third and fourth panels), where the collective effects of the observed mutations ultimately continue to push the population towards improving both traits. These rare mutants demonstrate that, at least on short evolutionary timescales, navigation of the performance space seems to be more driven by constraints imposed by the genetic wiring of the cell, which influences the relative

ease of improving one performance or the other, rather than fundamental or physiological constraints upon improving the performances themselves.

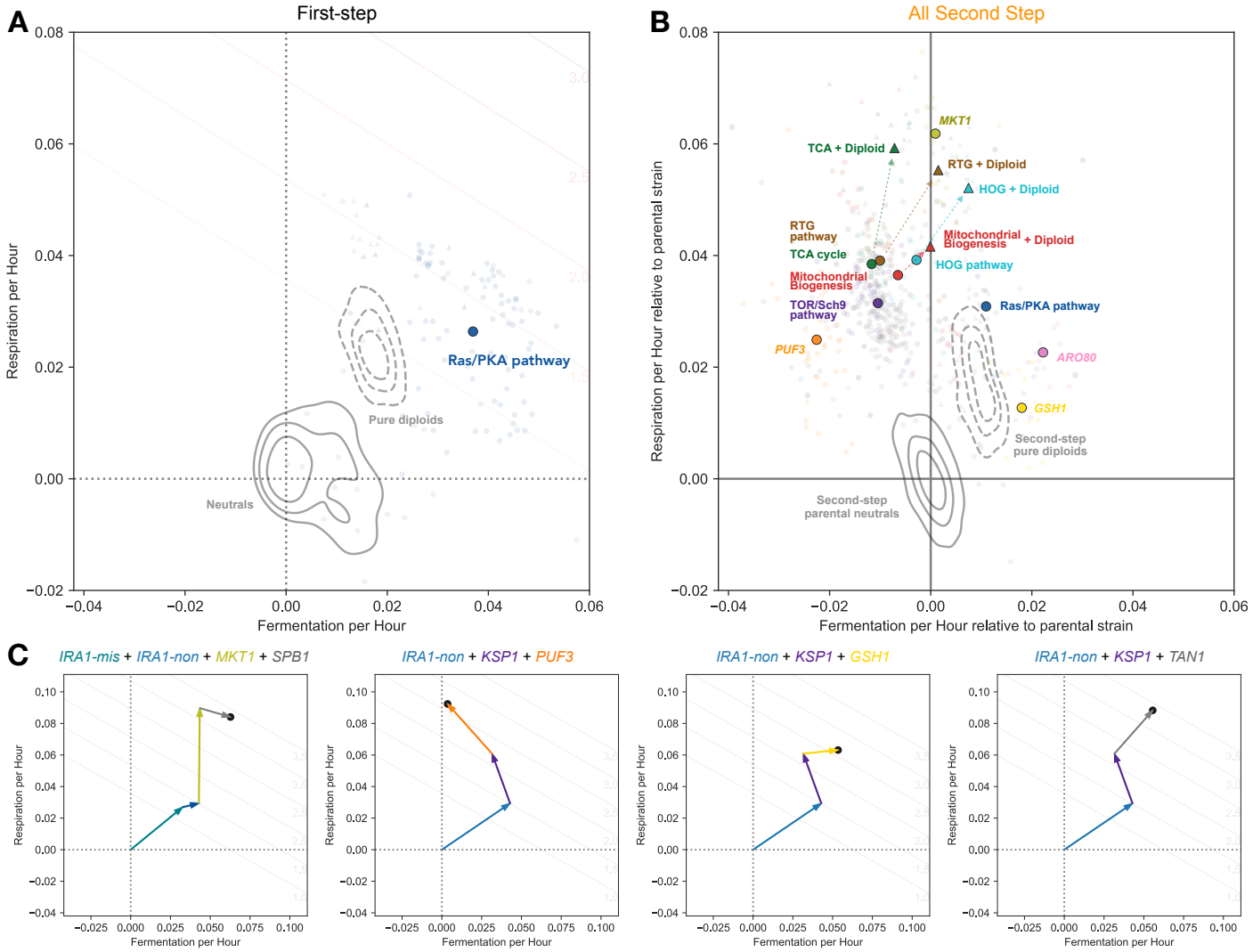

Figure 5. Adaptive modularity is driven by the accessibility of mutational targets that improve respiration at the cost of fermentation. (A) Ras/PKA and TOR/Sch9 mutants from the first-step of adaptation to improve both fermentation and respiration performance. **(B)** Most common second-step mutational targets tend to improve respiration at the cost of fermentation (centroids depicted as colored circles), except for rare Ras/PKA (blue), *ARO80* (pink), or *GSH1* (yellow) mutants; haploids shown as circles. Auto-diploids exhibit adaptive pleiotropy (dashed KDE estimate for all parental strains, colored by first-step mutation). Auto-diploidization is also adaptively pleiotropic on the background of other point mutations (triangles colored by pathway or gene category). Note that only centroids for each category of gene with at least 3 observed mutants were included. **(C)** Triple and quadruple mutants can ultimately drive adaptation towards adaptive pleiotropy (or adaptive modularity) despite being primarily composed of adaptively modular mutations. Note that the mutations beyond the first step are depicted in no particular order in these subpanels.

DISCUSSION

In this study, we sought to understand the frequent observation that single adaptive mutations observed in experimental evolution, especially those of large effect, can pleiotropically improve multiple distinct performances at once. This observation is puzzling because theoretical work suggests that as pleiotropy increases, large effect adaptive mutations should become less probable. This expected “cost of complexity” is the reason for why modularity is often seen as the necessary condition and the expected consequence of evolution of complex organisms by natural selection (Orr 2000; Welch and Waxman 2003; Wagner and Zhang 2011; Wagner, Pavlicev, and Cheverud 2007; Wagner and Altenberg 1996; Melo et al. 2016; Hartwell et al. 1999).

We focused on one striking example of pleiotropic adaptation that comes from previous studies of yeast evolving in a glucose-limited environment (Levy et al. 2015) in which 85% of the first-step single adaptive mutations improved performance in both fermentation and respiration growth phases (Fig1A, Fig3B) (Levy et al. 2015; Venkataram et al. 2016; Y. Li et al. 2018), despite these growth phases as being thought to be physiologically distinct.

Here, we investigated whether adaptation in the same low-glucose environment and 2-Day transfer as the original experiment (Levy et al. 2015) will continue following the path of adaptive pleiotropy (Fig. 1B) or will shift to become more modular (Fig. 1C). We thus further evolved 5 different first-step mutants, four in the Ras/PKA pathway *(IRA1-nonsense*, *IRA1-missense*, *CYR1*, and *GPB2*) and one in the Tor/Sch9 pathway (*TOR1*), sampled a large number of adaptive mutants, and evaluated their effects on the fermentation and respiration performances.

In all five cases, the results were qualitatively similar. First, adaptation proceeded to improve fitness, albeit to a somewhat muted degree. Second, while a number of mutants were adaptively pleiotropic, improving both fermentation and respiration performances, the dominant trend switched towards more modular adaptation. Specifically, nearly all adaptive mutants improved respiration performance sharply and many had no or only weakly positive or even negative effects on the fermentation performance (Fig. 3B). These results support a model of adaptation wherein early adaptation is driven by mutations of large effect that improve multiple performances at once. Then, after these mutations have become exhausted, adaptation may proceed via more modest mutations that improve performances in a stepwise manner (Figure 1C).

One remaining question is how pleiotropic adaptation is possible in the first place. The prevalence of the pleiotropic adaptation in the first step may be due to these mutations being primarily in Ras/PKA pathway genes. We thus hypothesized that the adaptive pleiotropy is a consequence of the way this pathway has evolved to shift rates of metabolism in both fermentation and respiration in a substantial, coordinated, and beneficial fashion (Wilson and Roach 2002). The notion is that even though these metabolic functions are distinct, they are

often required to be carried out in tandem, as respiration commonly follows fermentation for yeast. It is possible that sensing and signaling pathways such as the Ras/PKA pathway evolved to affect them together. This might be a general feature of signaling pathways as they must shift multiple functions and performances together and this ability then represents an attractive target for adaptive genetic changes.

If pleiotropic adaptation is a feature of the Ras/PKA pathway, the prediction is that 2nd step adaptive Ras/PKA pathway mutations will remain adaptively pleiotropic. This is indeed the case. Second-step mutations in the Ras/PKA pathway, mainly arising in the *TOR1* background, do improve both fermentation and respiration performances. A small number of second-step adaptive mutations outside of this pathway, in *ARO80* and *GSH1*, are also pleiotropically adaptive and improve both respiration and fermentation, but to a smaller degree than Ras/PKA pathway mutants. This suggests that the Ras/PKA pathway is virtually unique in its ability to modulate both fermentation and respiration performances together to a substantial degree in an adaptive manner, a notion also supported by the fact that we observe the shift towards modularity adaptation already in the second adaptive step.

A small number of adaptive clones in the second step improved both fermentation and respiration performances to a substantial degree. Sequencing of these clones showed that they acquired multiple mutations, and several of these clones improved both performances by the addition of two or more orthogonal steps. This suggests that adaptation can continue improving both performances but the adaptive walk needs to engage multiple modules and multiple mutations, making such adaptation slower than the first step of adaptation. This might be part of the reason why adaptation in general slows down over the course of evolution (Wiser, Ribeck, and Lenski 2013; Johnson et al. 2021; Good and Desai 2015; Aggeli, Li, and Sherlock 2021).

We argue that signaling pathways such as Ras/PKA have the capacity of generating “coherent pleiotropy”, where the output of many cellular processes can be affected without disrupting the proper regulation and function of each process. As such, signaling pathways that have been evolutionarily pre-wired to control combinations of selective pressures may be easily modified by mutation to coherently improve the performances under selection. The ability of signaling pathways to generate coherent pleiotropy implies that many adaptive mutations should hit signaling pathways. Indeed, this is what we see. For example, in cancer, the key oncogenes are located along cellular signaling pathways and engage either receptors of signals or represent key relay stations in these pathways (Bailey et al. 2018; Sanchez-Vega et al. 2018; Pawson and Warner 2007; Sondka et al. 2018; Hanahan and Weinberg 2011; Hanahan 2022).

On the other hand, this coherent pleiotropy of signaling pathways does not necessarily indicate that such mutations have no costs in other traits. Indeed, we see that many of the Ras/PKA mutants exhibit costs in stationary phase. Moreover, in previous work, we find that the Ras/PKA mutants have additional phenotypic effects with minor contributions to fitness in the Evo2D evolution condition but substantial effects in other conditions (Kinsler, Geiler-Samerotte, and

Petrov 2020). Thus, we might expect these signaling pathways to be most likely to be targeted by adaptation in relatively simple environments where the beneficial pleiotropic effects can be realized with only minor other costs.

In addition to cellular signaling pathways, other gene-regulatory, hormonal, and neuronal systems allow for organisms to be phenotypically plastic and involve coherent control of many traits of an organism. As such, these systems may also be attractive targets for evolutionary change, as they can serve as high-leverage routes for altering many traits simultaneously. The evolution of phenotypic plasticity hence paves the way for subsequent large-effect evolutionary shifts in local adaptation.

Finally, we believe that the existence of these high-leverage pleiotropic routes of adaptation must be incorporated into our thinking of the evolution of complex systems. Indeed, we commonly think of pleiotropy as purely random, with mutations shifting multiple traits at once in a random and thus largely incoherent way. This generates expectations that pleiotropy should be costly, as such incoherent shifts lead to a generically disorganized state. Given that actual organisms have low-dimensional but pleiotropic signaling and regulatory systems, pleiotropy can often be coherent and thus might often enhance adaptive potential and allow for surprisingly large-effect adaptive mutations. It is therefore important to think of regulation and adaptation as two sides of the same problem of how to change complex and tightly integrated systems in an adaptive manner.

REFERENCES

Aggeli, Dimitra, Yuping Li, and Gavin Sherlock. 2021. "Changes in the Distribution of Fitness Effects and Adaptive Mutational Spectra Following a Single First Step towards Adaptation." *Nature Communications* 12 (1): 5193. https://doi.org/10.1038/s41467-021-25440-7.

Ait-El-Mkadem, Samira, Manal Dayem-Quere, Mirjana Gusic, Annabelle Chaussenot, Sylvie Bannwarth, Bérengère François, Emmanuelle C. Genin, et al. 2017. "Mutations in MDH2, Encoding a Krebs Cycle Enzyme, Cause Early-Onset Severe Encephalopathy." *American Journal of Human Genetics* 100 (1): 151–59. https://doi.org/10.1016/j.ajhg.2016.11.014.

Altschul, S. F., W. Gish, W. Miller, E. W. Myers, and D. J. Lipman. 1990. "Basic Local Alignment Search Tool." *Journal of Molecular Biology* 215 (3): 403–10. https://doi.org/10.1016/S0022-2836(05)80360-2.

Bailey, Matthew H., Collin Tokheim, Eduard Porta-Pardo, Sohini Sengupta, Denis Bertrand, Amila Weerasinghe, Antonio Colaprico, et al. 2018. "Comprehensive Characterization of Cancer Driver Genes and Mutations." *Cell* 173 (2): 371–85.e18. https://doi.org/10.1016/j.cell.2018.02.060.

Bakerlee, Christopher W., Angela M. Phillips, Alex N. Nguyen Ba, and Michael M. Desai. 2021. "Dynamics and Variability in the Pleiotropic Effects of Adaptation in Laboratory Budding Yeast Populations." *eLife* 10 (October). https://doi.org/10.7554/eLife.70918.

BarcodeCounter2: Count DNA Barcodes Version 2. n.d. Github. Accessed April 10, 2024. https://github.com/sandeepvenkataram/BarcodeCounter2.

Blount, Zachary D., Christina Z. Borland, and Richard E. Lenski. 2008. "Historical Contingency and the Evolution of a Key Innovation in an Experimental Population of *Escherichia Coli*." *Proceedings of the National Academy of Sciences of the United States of America* 105 (23): 7899–7906. https://doi.org/10.1073/pnas.0803151105.

Boles Eckhard, de Jong-Gubbels Patricia, and Pronk Jack T. 1998. "Identification and Characterization ofMAE1, the Saccharomyces Cerevisiae Structural Gene Encoding Mitochondrial Malic Enzyme." *Journal of Bacteriology* 180 (11): 2875–82. https://doi.org/10.1128/jb.180.11.2875-2882.1998.

Bono, Lisa M., Leno B. Smith Jr, David W. Pfennig, and Christina L. Burch. 2017. "The Emergence of Performance Trade-Offs during Local Adaptation: Insights from Experimental Evolution." *Molecular Ecology* 26 (7): 1720–33. https://doi.org/10.1111/mec.13979.

Brown, James A., Gavin Sherlock, Chad L. Myers, Nicola M. Burrows, Changchun Deng, H. Irene Wu, Kelly E. McCann, Olga G. Troyanskaya, and J. Martin Brown. 2006. "Global Analysis of Gene Function in Yeast by Quantitative Phenotypic Profiling." *Molecular Systems Biology* 2 (January): 2006.0001. https://doi.org/10.1038/msb4100043.

Chaithanya, Koppisetty Viswa, and Himanshu Sinha. 2023. "MKT1 Alleles Regulate Stress Responses through Posttranscriptional Modulation of Puf3 Targets in Budding Yeast." *Yeast* 40 (12): 616–27. https://doi.org/10.1002/yea.3908.

Chang, Yeonji, and Won-Ki Huh. 2018. "Ksp1-Dependent Phosphorylation of eIF4G Modulates Post-Transcriptional Regulation of Specific mRNAs under Glucose Deprivation Conditions." *Nucleic Acids Research* 46 (6): 3047–60. https://doi.org/10.1093/nar/gky097.

Chou, Hsin-Hung, Hsuan-Chao Chiu, Nigel F. Delaney, Daniel Segrè, and Christopher J. Marx. 2011. "Diminishing Returns Epistasis among Beneficial Mutations Decelerates Adaptation." *Science* 332 (6034): 1190–92. https://doi.org/10.1126/science.1203799.

Cingolani, Pablo, Adrian Platts, Le Lily Wang, Melissa Coon, Tung Nguyen, Luan Wang, Susan J. Land, Xiangyi Lu, and Douglas M. Ruden. 2012. "A Program for Annotating and Predicting the Effects of Single Nucleotide Polymorphisms, SnpEff: SNPs in the Genome of Drosophila Melanogaster Strain w1118; Iso-2; Iso-3." *Fly* 6 (2): 80–92. https://doi.org/10.4161/fly.19695.

DeRisi, J. L., V. R. Iyer, and P. O. Brown. 1997. "Exploring the Metabolic and Genetic Control of Gene Expression on a Genomic Scale." *Science* 278 (5338): 680–86. https://doi.org/10.1126/science.278.5338.680.

Fisher, Kaitlin J., Sean W. Buskirk, Ryan C. Vignogna, Daniel A. Marad, and Gregory I. Lang. 2018. "Adaptive Genome Duplication Affects Patterns of Molecular Evolution in Saccharomyces Cerevisiae." *PLoS Genetics* 14 (5): e1007396. https://doi.org/10.1371/journal.pgen.1007396.

Good, Benjamin H., and Michael M. Desai. 2015. "The Impact of Macroscopic Epistasis on Long-Term

Evolutionary Dynamics." *Genetics* 199 (1): 177–90. https://doi.org/10.1534/genetics.114.172460.
Gupta, Saumya, Aparna Radhakrishnan, Pandu Raharja-Liu, Gen Lin, Lars M. Steinmetz, Julien Gagneur, and Himanshu Sinha. 2015. "Temporal Expression Profiling Identifies Pathways Mediating Effect of Causal Variant on Phenotype." *PLoS Genetics* 11 (6): e1005195. https://doi.org/10.1371/journal.pgen.1005195.
Hanahan, Douglas. 2022. "Hallmarks of Cancer: New Dimensions." *Cancer Discovery* 12 (1): 31–46. https://doi.org/10.1158/2159-8290.CD-21-1059.
Hanahan, Douglas, and Robert A. Weinberg. 2011. "Hallmarks of Cancer: The next Generation." *Cell* 144 (5): 646–74. https://doi.org/10.1016/j.cell.2011.02.013.
Harms, Michael J., and Joseph W. Thornton. 2014. "Historical Contingency and Its Biophysical Basis in Glucocorticoid Receptor Evolution." *Nature* 512 (7513): 203–7. https://doi.org/10.1038/nature13410.
Hartwell, L. H., J. J. Hopfield, S. Leibler, and A. W. Murray. 1999. "From Molecular to Modular Cell Biology." *Nature* 402 (6761 Suppl): C47–52. https://doi.org/10.1038/35011540.
Hong, Jungeui, and David Gresham. 2014. "Molecular Specificity, Convergence and Constraint Shape Adaptive Evolution in Nutrient-Poor Environments." *PLoS Genetics* 10 (1): e1004041. https://doi.org/10.1371/journal.pgen.1004041.
Iraqui, I., S. Vissers, B. André, and A. Urrestarazu. 1999. "Transcriptional Induction by Aromatic Amino Acids in Saccharomyces Cerevisiae." *Molecular and Cellular Biology* 19 (5): 3360–71. https://doi.org/10.1128/MCB.19.5.3360.
Jasmin, Jean-Nicolas, and Rees Kassen. 2007. "On the Experimental Evolution of Specialization and Diversity in Heterogeneous Environments." *Ecology Letters* 10 (4): 272–81. https://doi.org/10.1111/j.1461-0248.2007.01021.x.
Johnson, Milo S., Shreyas Gopalakrishnan, Juhee Goyal, Megan E. Dillingham, Christopher W. Bakerlee, Parris T. Humphrey, Tanush Jagdish, et al. 2021. "Phenotypic and Molecular Evolution across 10,000 Generations in Laboratory Budding Yeast Populations." *eLife* 10 (January). https://doi.org/10.7554/eLife.63910.
Kinsler, Grant, Kerry Geiler-Samerotte, and Dmitri A. Petrov. 2020. "Fitness Variation across Subtle Environmental Perturbations Reveals Local Modularity and Global Pleiotropy of Adaptation." *eLife* 9 (December). https://doi.org/10.7554/eLife.61271.
Kinsler, Grant, Kara Schmidlin, Daphne Newell, Rachel Eder, Sam Apodaca, Grace Lam, Dmitri Petrov, and Kerry Geiler-Samerotte. 2023. "Extreme Sensitivity of Fitness to Environmental Conditions: Lessons from #1BigBatch." *Journal of Molecular Evolution* 91 (3): 293–310. https://doi.org/10.1007/s00239-023-10114-3.
Kistler, M., K. Maier, and F. Eckardt-Schupp. 1990. "Genetic and Biochemical Analysis of Glutathione-Deficient Mutants of Saccharomyces Cerevisiae." *Mutagenesis* 5 (1): 39–44. https://doi.org/10.1093/mutage/5.1.39.
Komeili, A., K. P. Wedaman, E. K. O'Shea, and T. Powers. 2000. "Mechanism of Metabolic Control. Target of Rapamycin Signaling Links Nitrogen Quality to the Activity of the Rtg1 and Rtg3 Transcription Factors." *The Journal of Cell Biology* 151 (4): 863–78. https://doi.org/10.1083/jcb.151.4.863.
Kryazhimskiy, Sergey, Daniel P. Rice, Elizabeth R. Jerison, and Michael M. Desai. 2014. "Microbial Evolution. Global Epistasis Makes Adaptation Predictable despite Sequence-Level Stochasticity." *Science* 344 (6191): 1519–22. https://doi.org/10.1126/science.1250939.
Kurita, O., and Y. Nishida. 1999. "Involvement of Mitochondrial Aldehyde Dehydrogenase ALD5 in Maintenance of the Mitochondrial Electron Transport Chain in Saccharomyces Cerevisiae." *FEMS Microbiology Letters* 181 (2): 281–87. https://doi.org/10.1111/j.1574-6968.1999.tb08856.x.
Langmead, Ben, and Steven L. Salzberg. 2012. "Fast Gapped-Read Alignment with Bowtie 2." *Nature Methods* 9 (4): 357–59. https://doi.org/10.1038/nmeth.1923.
Lapointe, Christopher P., Jonathan A. Stefely, Adam Jochem, Paul D. Hutchins, Gary M. Wilson, Nicholas W. Kwiecien, Joshua J. Coon, Marvin Wickens, and David J. Pagliarini. 2018. "Multi-Omics Reveal Specific Targets of the RNA-Binding Protein Puf3p and Its Orchestration of Mitochondrial Biogenesis." *Cell Systems* 6 (1): 125–35.e6. https://doi.org/10.1016/j.cels.2017.11.012.
Lee, Chien-Der, and Benjamin P. Tu. 2015. "Glucose-Regulated Phosphorylation of the PUF Protein Puf3

Regulates the Translational Fate of Its Bound mRNAs and Association with RNA Granules." *Cell Reports* 11 (10): 1638–50. https://doi.org/10.1016/j.celrep.2015.05.014.

Lee, Kyusung, and Ji-Sook Hahn. 2013. "Interplay of Aro80 and GATA Activators in Regulation of Genes for Catabolism of Aromatic Amino Acids in Saccharomyces Cerevisiae." *Molecular Microbiology* 88 (6): 1120–34. https://doi.org/10.1111/mmi.12246.

Levy, Sasha F., Jamie R. Blundell, Sandeep Venkataram, Dmitri A. Petrov, Daniel S. Fisher, and Gavin Sherlock. 2015. "Quantitative Evolutionary Dynamics Using High-Resolution Lineage Tracking." *Nature* 519 (7542): 181–86. https://doi.org/10.1038/nature14279.

Liao, X., and R. A. Butow. 1993. "RTG1 and RTG2: Two Yeast Genes Required for a Novel Path of Communication from Mitochondria to the Nucleus." *Cell* 72 (1): 61–71. https://doi.org/10.1016/0092-8674(93)90050-z.

Li, Fangfei, Aditya Mahadevan, and Gavin Sherlock. 2023. "An Improved Algorithm for Inferring Mutational Parameters from Bar-Seq Evolution Experiments." *BMC Genomics* 24 (1): 246. https://doi.org/10.1186/s12864-023-09345-x.

Li, Fangfei, Jason Tarkington, and Gavin Sherlock. 2023. "Fit-Seq2.0: An Improved Software for High-Throughput Fitness Measurements Using Pooled Competition Assays." *Journal of Molecular Evolution* 91 (3): 334–44. https://doi.org/10.1007/s00239-023-10098-0.

Li, Heng. 2011. "A Statistical Framework for SNP Calling, Mutation Discovery, Association Mapping and Population Genetical Parameter Estimation from Sequencing Data." *Bioinformatics* 27 (21): 2987–93. https://doi.org/10.1093/bioinformatics/btr509.

Li, Heng, and Richard Durbin. 2009. "Fast and Accurate Short Read Alignment with Burrows–Wheeler Transform." *Bioinformatics* 25 (14): 1754–60. https://doi.org/10.1093/bioinformatics/btp324.

Liu, Zhengchang, Takayuki Sekito, Mário Spírek, Janet Thornton, and Ronald A. Butow. 2003. "Retrograde Signaling Is Regulated by the Dynamic Interaction between Rtg2p and Mks1p." *Molecular Cell* 12 (2): 401–11. https://doi.org/10.1016/s1097-2765(03)00285-5.

Li, Yuping, Dmitri A. Petrov, and Gavin Sherlock. 2019. "Single Nucleotide Mapping of Trait Space Reveals Pareto Fronts That Constrain Adaptation." *Nature Ecology & Evolution* 3 (11): 1539–51. https://doi.org/10.1038/s41559-019-0993-0.

Li, Yuping, Sandeep Venkataram, Atish Agarwala, Barbara Dunn, Dmitri A. Petrov, Gavin Sherlock, and Daniel S. Fisher. 2018. "Hidden Complexity of Yeast Adaptation under Simple Evolutionary Conditions." *Current Biology: CB* 28 (4): 515–25.e6. https://doi.org/10.1016/j.cub.2018.01.009.

McAlister-Henn, L., and L. M. Thompson. 1987. "Isolation and Expression of the Gene Encoding Yeast Mitochondrial Malate Dehydrogenase." *Journal of Bacteriology* 169 (11): 5157–66. https://doi.org/10.1128/jb.169.11.5157-5166.1987.

Melo, Diogo, Arthur Porto, James M. Cheverud, and Gabriel Marroig. 2016. "Modularity: Genes, Development and Evolution." *Annual Review of Ecology, Evolution, and Systematics* 47 (September): 463–86. https://doi.org/10.1146/annurev-ecolsys-121415-032409.

Murphy, J. Patrick, Ekaterina Stepanova, Robert A. Everley, Joao A. Paulo, and Steven P. Gygi. 2015. "Comprehensive Temporal Protein Dynamics during the Diauxic Shift in Saccharomyces Cerevisiae." *Molecular & Cellular Proteomics: MCP* 14 (9): 2454–65. https://doi.org/10.1074/mcp.M114.045849.

Navarro-Aviño, J. P., R. Prasad, V. J. Miralles, R. M. Benito, and R. Serrano. 1999. "A Proposal for Nomenclature of Aldehyde Dehydrogenases in Saccharomyces Cerevisiae and Characterization of the Stress-Inducible ALD2 and ALD3 Genes." *Yeast* 15 (10A): 829–42. https://doi.org/10.1002/(SICI)1097-0061(199907)15:10A<829::AID-YEA423>3.0.CO;2-9.

Orr, H. A. 2000. "Adaptation and the Cost of Complexity." *Evolution; International Journal of Organic Evolution* 54 (1): 13–20. https://doi.org/10.1111/j.0014-3820.2000.tb00002.x.

Park, Yeonwoo, Brian P. H. Metzger, and Joseph W. Thornton. 2022. "Epistatic Drift Causes Gradual Decay of Predictability in Protein Evolution." *Science* 376 (6595): 823–30. https://doi.org/10.1126/science.abn6895.

Pawson, T., and N. Warner. 2007. "Oncogenic Re-Wiring of Cellular Signaling Pathways." *Oncogene* 26 (9): 1268–75. https://doi.org/10.1038/sj.onc.1210255.

Reinders, Jörg, Karina Wagner, Rene P. Zahedi, Diana Stojanovski, Beate Eyrich, Martin van der Laan, Peter Rehling, Albert Sickmann, Nikolaus Pfanner, and Chris Meisinger. 2007. "Profiling

962 Phosphoproteins of Yeast Mitochondria Reveals a Role of Phosphorylation in Assembly of the ATP
963 Synthase*." *Molecular & Cellular Proteomics: MCP* 6 (11): 1896–1906.
964 https://doi.org/10.1074/mcp.M700098-MCP200.
965 Repetto, B., and A. Tzagoloff. 1989. "Structure and Regulation of KGD1, the Structural Gene for Yeast
966 Alpha-Ketoglutarate Dehydrogenase." *Molecular and Cellular Biology* 9 (6): 2695–2705.
967 https://doi.org/10.1128/mcb.9.6.2695-2705.1989.
968 Sanchez-Vega, Francisco, Marco Mina, Joshua Armenia, Walid K. Chatila, Augustin Luna, Konnor C. La,
969 Sofia Dimitriadoy, et al. 2018. "Oncogenic Signaling Pathways in The Cancer Genome Atlas." *Cell*
970 173 (2): 321–37.e10. https://doi.org/10.1016/j.cell.2018.03.035.
971 Schlossarek, Dennis, Marcin Luzarowski, Ewelina M. Sokołowska, Venkatesh P. Thirumalaikumar, Lisa
972 Dengler, Lothar Willmitzer, Jennifer C. Ewald, and Aleksandra Skirycz. 2022. "Rewiring of the
973 Protein-Protein-Metabolite Interactome during the Diauxic Shift in Yeast." *Cellular and Molecular Life*
974 *Sciences: CMLS* 79 (11): 550. https://doi.org/10.1007/s00018-022-04569-8.
975 Sekito, Takayuki, Zhengchang Liu, Janet Thornton, and Ronald A. Butow. 2002. "RTG-Dependent
976 Mitochondria-to-Nucleus Signaling Is Regulated by MKS1 and Is Linked to Formation of Yeast Prion
977 [URE3]." *Molecular Biology of the Cell* 13 (3): 795–804. https://doi.org/10.1091/mbc.01-09-0473.
978 Sekito, T., J. Thornton, and R. A. Butow. 2000. "Mitochondria-to-Nuclear Signaling Is Regulated by the
979 Subcellular Localization of the Transcription Factors Rtg1p and Rtg3p." *Molecular Biology of the Cell*
980 11 (6): 2103–15. https://doi.org/10.1091/mbc.11.6.2103.
981 Sondka, Zbyslaw, Sally Bamford, Charlotte G. Cole, Sari A. Ward, Ian Dunham, and Simon A. Forbes.
982 2018. "The COSMIC Cancer Gene Census: Describing Genetic Dysfunction across All Human
983 Cancers." *Nature Reviews. Cancer* 18 (11): 696–705. https://doi.org/10.1038/s41568-018-0060-1.
984 Suissa, M., K. Suda, and G. Schatz. 1984. "Isolation of the Nuclear Yeast Genes for Citrate Synthase and
985 Fifteen Other Mitochondrial Proteins by a New Screening Method." *The EMBO Journal* 3 (8): 1773–
986 81. https://doi.org/10.1002/j.1460-2075.1984.tb02045.x.
987 Tung, Sudipta, Christopher W. Bakerlee, Angela M. Phillips, Alex N. Nguyen Ba, and Michael M. Desai.
988 2021. "The Genetic Basis of Differential Autodiploidization in Evolving Yeast Populations." *G3* 11 (8).
989 https://doi.org/10.1093/g3journal/jkab192.
990 Umekawa, Midori, and Daniel J. Klionsky. 2012. "Ksp1 Kinase Regulates Autophagy via the Target of
991 Rapamycin Complex 1 (TORC1) Pathway." *The Journal of Biological Chemistry* 287 (20): 16300–
992 310. https://doi.org/10.1074/jbc.M112.344952.
993 Van der Auwera, Geraldine A., and Brian D. O'Connor. 2020. *Genomics in the Cloud: Using Docker,*
994 *GATK, and WDL in Terra*. "O'Reilly Media, Inc."
995 https://play.google.com/store/books/details?id=vsXaDwAAQBAJ.
996 Venkataram, Sandeep, Barbara Dunn, Yuping Li, Atish Agarwala, Jessica Chang, Emily R. Ebel, Kerry
997 Geiler-Samerotte, et al. 2016. "Development of a Comprehensive Genotype-to-Fitness Map of
998 Adaptation-Driving Mutations in Yeast." *Cell* 166 (6): 1585–96.e22.
999 https://doi.org/10.1016/j.cell.2016.08.002.
1000 Wagner, Günter P., and Lee Altenberg. 1996. "PERSPECTIVE: COMPLEX ADAPTATIONS AND THE
1001 EVOLUTION OF EVOLVABILITY." *Evolution; International Journal of Organic Evolution* 50 (3): 967–
1002 76. https://doi.org/10.1111/j.1558-5646.1996.tb02339.x.
1003 Wagner, Günter P., Mihaela Pavlicev, and James M. Cheverud. 2007. "The Road to Modularity." *Nature*
1004 *Reviews. Genetics* 8 (12): 921–31. https://doi.org/10.1038/nrg2267.
1005 Wagner, Günter P., and Jianzhi Zhang. 2011. "The Pleiotropic Structure of the Genotype-Phenotype Map:
1006 The Evolvability of Complex Organisms." *Nature Reviews. Genetics* 12 (3): 204–13.
1007 https://doi.org/10.1038/nrg2949.
1008 Welch, John J., and David Waxman. 2003. "Modularity and the Cost of Complexity." *Evolution;*
1009 *International Journal of Organic Evolution* 57 (8): 1723–34. https://doi.org/10.1111/j.0014-
1010 3820.2003.tb00581.x.
1011 Wilson, Wayne A., and Peter J. Roach. 2002. "Nutrient-Regulated Protein Kinases in Budding Yeast."
1012 *Cell* 111 (2): 155–58. https://doi.org/10.1016/s0092-8674(02)01043-7.
1013 Wiser, Michael J., Noah Ribeck, and Richard E. Lenski. 2013. "Long-Term Dynamics of Adaptation in
1014 Asexual Populations." *Science* 342 (6164): 1364–67. https://doi.org/10.1126/science.1243357.

1015 Wünsche, Andrea, Duy M. Dinh, Rebecca S. Satterwhite, Carolina Diaz Arenas, Daniel M. Stoebel, and
1016 Tim F. Cooper. 2017. “Diminishing-Returns Epistasis Decreases Adaptability along an Evolutionary
1017 Trajectory.” *Nature Ecology & Evolution* 1 (4): 61. https://doi.org/10.1038/s41559-016-0061.
1018 Zampar, Guillermo G., Anne Kümmel, Jennifer Ewald, Stefan Jol, Bastian Niebel, Paola Picotti, Ruedi
1019 Aebersold, Uwe Sauer, Nicola Zamboni, and Matthias Heinemann. 2013. “Temporal System-Level
1020 Organization of the Switch from Glycolytic to Gluconeogenic Operation in Yeast.” *Molecular Systems*
1021 *Biology* 9: 651. https://doi.org/10.1038/msb.2013.11.

METHODS

Constructing barcoded populations from first-step mutants

To conduct second-step evolution experiments, we constructed barcoded populations for each of five mutations (see table 1) that arose in the original 2-Day evolution experiment (Levy et al. 2015). Construction of the barcoded populations of *CYR1, GPB2,* and *TOR1* mutations was previously described (Aggeli, Li, and Sherlock 2021). To barcode *IRA1-nonsense* and *IRA1-missense* mutants, we followed a similar procedure. Specifically, we backcrossed the *IRA1* mutants (*MATα*) to GSY5375, a *MATa* ancestral S288C strain that harbors the pre-landing pad locus (Aggeli, Li, and Sherlock 2021). After sporulation and tetrad dissection, we performed Sanger sequencing to identify segregants that were *MAT*α, carried the *IRA1* variant of interest, and the pre-landing pad allele at the barcode locus, ensuring the removal of the barcode initially labeling this strain. These segregants were used for downstream transformation of barcodes.

We then barcoded these strains with a low and high complexity barcode as described in Aggeli et al. We first transformed in the low-complexity barcode by PCR-amplifying a region from the L001 library, which harbors a NatMX selectable marker, half of *URA3*, an artificial intron, a low-complexity barcode sequence, and a lox66 site. We then selected for successful transformants using YPD + Nat plates and isolated 4 and 8 colonies for *IRA1-missense* and *IRA1-nonsense* strains, respectively, each with a unique low-complexity barcode. For each of these strains, we then transformed a library of high-complexity barcodes (pBAR3). After transformation, cells were grown in YP + 2% galactose for 16hrs to induce Cre recombinase expression prior to selection on SC-ura plates with 2% glucose. We then estimated the number of unique transformants by counting the number of colonies grown from plating a dilution. We additionally estimated the relative number of unique transformants by amplicon Illumina sequencing using the sequencing primers described below.

To construct populations for evolution experiments, we pooled together transformants from multiple high-complexity transformations, such that each barcode was equally represented in each pool. This resulted in pools of ~100,000 high-complexity barcodes for each evolution experiment with the exception of Evo2D *IRA1-missense* evolution pool which contained ~40,000 high-complexity barcodes. Transformants were pooled such that each low-complexity barcode was only present in one evolution pool, allowing us later to identify evolution conditions based on the identity of the low-complexity barcode. For Evo1D experiments, a pool of *IRA1-missense* and *IRA1-nonsense* transformants was used, containing equal numbers in abundance, albeit with ~32,000 unique *IRA1-missense* barcodes and ~60,000 *IRA1-nonsense* barcodes. A single pool that contained barcoded populations of *CYR1*, *GPB2*, and *TOR1* mutants was used for the second-step Evo1D and Evo3D experiments for these genotypes.

Conducting evolution experiments.

We conducted evolution experiments with barcoded populations under identical conditions to the original evolution experiment. Briefly, ~10^8 cells of each evolution population pool was

inoculated in 50 mL of SC-ura + 2% dextrose + hygromycin in 500 mL Delong flasks and grown overnight at 30°C with shaking at 223 rpm. 500 µL of saturated overnight culture was then transferred to 100 mL of glucose-limited M3 medium (5x delft medium with 4% ammonium sulfate and 1.5% dextrose) in 500 mL Delong flasks for the evolution experiment. For most of the evolution experiments, the culture was split into 2 replicate flasks at this point. Second-step Evo3D experiments from *IRA1-missense* or *IRA1-nonsense* mutants used 3 replicates each. Cultures then propagated every 24, 48, or 72 hours for Evo1D, Evo2D, and Evo3D conditions, respectively. At the time of transfer, a set volume was transferred into 100 mL of fresh medium. In order to keep the bottleneck size consistent at ~5x10^7 viable cells, the volume varied by condition. Evo2D conditions used 400 µl of transfer volume. Evo1D and Evo3D conditions used 500 µL of transfer volume, which accounted for decreased cell density and decreased cell viability in these conditions, respectively. Two 1 mL volumes of saturated culture were frozen as glycerol stocks. The remaining culture was spun down, resuspended in 5 mL of sorbitol freezing solution (0.9M sorbitol, 100mM Tris pH 7.5, 100mM EDTA) and frozen at -20°C for subsequent genomic DNA extraction and barcode library sequencing preparation.

Isolation of clones from evolution experiments.

To isolate clones for fitness measurement experiments, quantification of growth phase performances, and whole genome sequencing, we sorted individual cells as previously described (Y. Li, Petrov, and Sherlock 2019) . Specifically, we sorted 480 individual cells (five 96-well plates) from each replicate evolution experiment into single wells of a 96-well plate with 100 µL of YPD medium. This resulted in a total of 80 plates (~7,680 sorted cells) across the 16 evolution experiments. Sorted cells were then grown at 30°C for 3 days without shaking until the cells reached saturation. Saturated cultures (5µl) were then transferred to deep-well 96-well plates with 300 µL of YPD. After 2 days of growth at 30°C without shaking, 100 µL of culture were mixed with glycerol and frozen at -80°C. 20 µL of saturated culture were transferred to 96-well PCR plates and frozen at -20°C. for barcode identification. Saturated culture was also plated onto Benomyl plates to assay ploidy (Venkataram et al. 2016).

Barcode identification by Metagrid.

To identify the barcode associated with each well and ensure that multiple clones with the same barcode were not kept for downstream fitness measurement experiments, we performed sequencing on the barcodes of the clones in each well. Saturated culture (20µl) was transferred to 96-well plates and frozen at -20°C. Cells were then lysed by incubation at 95°C for 15 min. 5 µL of lysed culture were used as the template for PCR amplification of the barcode region. We performed two steps of PCR. In the first-step of PCR, we used a set of 72 forward and 64 reverse first-step primers, each with a unique 8-bp multiplexing tag, to combinatorially label each well. After the first-step of PCR, 5 µL of each well's PCR product from 5 plates was pooled together and the appropriate 250bp band was isolated using gel purification. A second-step of PCR was then performed with standard Nextera primers. Amplicon libraries were then sequenced on Illumina MiSeq or HiSeq machines.

To computationally identify the barcodes associated with each well, we used BarcodeCounter2 to extract the multiplexing indexes and barcode regions from each read. We then associated barcodes with each well by taking the barcode with the most reads per well, provided the well had at least 200 reads, the barcode was at least 60% of the well's reads, and it received more than 1.5x the second-highest barcode in the well. This resulted in identifying the locations of 1785 unique barcoded clones. This is lower than the highest possible number of 7,680 clones due to a combination of some wells receiving multiple clones, multiple wells receiving cells of the same barcode, and drop out due to sequencing depth. To further validate our approach, we randomly selected 3 wells per plate and performed Sanger sequencing of their barcodes. Of the wells where both barcodes were identified using the metagrid approach and Sanger reads were of sufficiently high quality, over 85% of the barcodes matched. We subsequently pooled each uniquely barcoded clone by evolution condition and parental strain, resulting in 4 pools of barcoded lineages to be used for fitness measurement experiments.

Benomyl ploidy test.

To characterize the ploidy of each sorted clone, we performed a high-throughput ploidy test that was previously developed (Venkataram et al. 2016). Saturated culture from cell sorting was pinned onto YPD agar plates containing 20 mg/mL benomyl. Plates were then grown at 25°C for 2 days and then imaged. Clones with inhibited growth on the benomyl medium were identified as diploids. Clones with normal growth on the benomyl medium were identified as haploids. See "Mutation and ploidy classification" section below.

Constructing barcoded pools

To construct a pool of lineages for fitness measurement experiments, we generated one large pool of barcoded lineages isolated from previous evolution experiments and the evolution experiments described in this study. Briefly, one tube of each barcode pool was thawed and grown in YPD at 30°C overnight. After the overnight growth, we pooled all barcode-sub pools together, adjusting for the number of barcodes in each pool and the OD600 of the culture, such that each barcode was equally represented in this big pool. This big pool was then split into 1 mL glycerol stock aliquots and frozen at -80°C.

To precisely measure the mean fitness of the population, we constructed two pools of 60 neutral lineages from Venkataram 2016 and Li 2019. Briefly, we identified barcodes that exhibited neutral fitness estimates across all previous experiments done with these pools of barcoded lineages (Venkataram et al. 2016; Y. Li et al. 2018; Y. Li, Petrov, and Sherlock 2019; Kinsler, Geiler-Samerotte, and Petrov 2020). We then streaked out from glycerol stocks onto YPD plates. A single colony was picked from each barcoded lineage and grown in 96-well deep-well plates for 2 days. Wells for each collection of 60 neutrals were then pooled equally by volume. Then, glycerol stocks were created with 1 mL of pooled culture and frozen at -80°C.

Fitness measurement experiments

To quantify fitness effects, we performed fitness measurement experiments. We streaked out DPY256 (an ancestor strain which harbors an ApaLI restriction site in the barcode region) onto a YPD plate. After two days of growth, a colony was picked and grown up in 50 mL of YPD overnight. Additionally, one tube each of the 60-neutral pool from Venkataram 2016 and one tube of the 60-neutral pool from the Li 2019 pool was thawed and grown separately in 50 mL of YPD overnight.

5x10^7 cells from DPY256 ancestor, each of the two neutral pools, and the big pool (see Constructing barcoded pools) were then separately inoculated into four 500 mL Delong flasks containing 100 mL of M3 medium for one cycle of pre-culture in the selective condition. This resulted in a total of 16 flasks of culture, corresponding to each set of barcoded cells and the four conditions.

After one cycle of growth (which corresponded to 24h for the 1-Day transfer condition, 48h for 2-Day, 72h for 3-Day, and 120h for 5-Day), the cultures were pooled by volume such that the big pool of barcoded lineages represented 2% or 5% of the population. In the 2% flasks, 2% of the population was the big pool of evolved lineages, 2% were Venkataram 2016 neutrals, 2% were Li 2019 neutrals, and 94% of the population was DPY256 ancestor. In the 5% flasks, 5% of the population was the big pool of evolved lineages, 2% were Venkataram 2016 neutrals, 2% were Li 2019 neutrals, and 91% of the population was DPY256 ancestor. These pools of lineages is considered “Timepoint 0” for each condition and pooling percentage.

We then transferred a set volume of this pool to replicate flasks (2 replicates for 1- and 2-Day experiments, 3 replicates for 3- and 5-Day experiments) containing 100 mL M3 medium such that ~5x10^7 of viable cells were transferred. This volume was 500 µL for 1-, 3-, and 5-Day experiments and 400 µL for 2-Day experiments. The culture was then grown at 30°C in an incubator shaking at 223 RPM. After the set amount of time corresponding to each condition, a fixed volume of culture (500 µL for 1-, 3-, and 5-Day experiments and 400 µL for 2-Day experiments) to fresh 100 mL of M3 medium in 500 mL DeLong flasks. This serial dilution was continued for until transfer 6 for 1- and 2-Day experiments and until transfer 2 for 3- and 5-Day experiments.

After each transfer, the remaining culture was frozen for downstream DNA extraction, barcode amplification, and sequencing. To freeze the culture, we transferred the culture to 50 mL conical tubes, spun down at 3000 rpm for 5 min, resuspending in 5 mL sorbitol freezing solution (0.9 M sorbitol, 0.1 M Tris-HCL pH 7.5, 0.1 M EDTA pH 8.0), aliquoted into three 1.5 mL tubes, and stored at −80°C.

Genomic DNA extraction

Genomic DNA was extracted from frozen cells as described previously (Aggeli, Li, and Sherlock 2021). Briefly, 400 µL of frozen cells in sorbitol solution was spun down at 3500 rpm for 3 min. After discarding the supernatant, the cell pellet was then washed in 400 µL of sterile water and spun down at 3500 rpm for 3 min and the supernatant was discarded. The cell pellet was then re-suspended in 400 µL of extraction buffer (0.9 M sorbitol, 50 mM Na phosphate pH 7.5, 240 µg/mL zymolase, 14 mM β-mercaptoethanol) and incubated at 37°C for 30min. We then added 40 µL of 0.5 M EDTA, 40 µL of 10% SDS, and 56 µL of proteinase K (Life Technologies 25530-015), vortexing after each addition. The mixture was then incubated at 65°C for 30 min. After the incubation, tubes were placed on ice for 5 min and then 200 µL of 5 M potassium acetate were added and tubes were shaken to mix. Following a 30 min incubation on ice, the samples were spun for 10 min at 17,000 rpm. The supernatant was transferred to a new 1.5 mL tube containing 750 µL of isopropanol and placed on ice for 5 min. We then spun the samples at 17,000 rpm for 10min and discarded the supernatant. The DNA pellet was then washed twice with 750 µL 70% ethanol, each time vortexing very briefly, spun at 17,000 rpm for 2 min, and discarding the supernatant. After allowing the DNA pellet to dry completely, it was resuspended in 50 µl 10 mM Tris ph 7.5 or 50 µL nuclease free water. We then added 1 µL of 20 mg/mL RNase A and subsequently incubated at 65°C for 30 min. DNA was then quantified using the Qubit Range dsDNA assay kit.

Restriction digest of ancestral strain's barcode

Because over 90% of the initial population during the fitness measurement experiments consists of the ancestral strain, we sought to reduce the proportion of reads that represented its barcode to reduce sequencing costs. We thus performed restriction digestion using the ApaLI restriction site (GTGCAC) engineered into the barcode region of the DPY256 ancestral strain on DNA for each sample prior to (and following) PCR amplification. We added 1 µL of ApaLI (NEB #R0507L) and 5.5 µL of Cutsmart Buffer (NEB #R0507L) to genomic DNA and incubated at 37°C for at least 1hr. Note that no barcode strains besides the ancestral strain contain this restriction site, due to the design of the barcode region.

Barcode sequencing library preparation

To prepare sequencing libraries of the barcodes, we used a two-step PCR amplification protocol, as previously described (Venkataram et al. 2016; Kinsler, Geiler-Samerotte, and Petrov 2020; Y. Li et al. 2018). In the first step of PCR, we use HPLC-purified primers that contain "inline indices" to label samples and 8-bp Unique Molecular Identifiers (UMIs) to identify barcode reads from the same yeast cell that have been sequenced multiple times due to PCR amplification.

Step 1 forward primers:

F201	TCGTCGGCAGCGTC AGATGTGTATAAGAGACAG (N1:25252525)(N1)(N1) (N1)(N1)(N1) (N1)(N1)CGATGTT TAATATGGACTAAAGGAGGCTTTT
F202	TCGTCGGCAGCGTC AGATGTGTATAAGAGACAG (N1:25252525)(N1)(N1) (N1)(N1)(N1) (N1)(N1)ACAGTGT TAATATGGACTAAAGGAGGCTTTT
F203	TCGTCGGCAGCGTC AGATGTGTATAAGAGACAG (N1:25252525)(N1)(N1) (N1)(N1)(N1) (N1)(N1)TGACCAT TAATATGGACTAAAGGAGGCTTTT
F204	TCGTCGGCAGCGTC AGATGTGTATAAGAGACAG (N1:25252525)(N1)(N1) (N1)(N1)(N1) (N1)(N1)GCCAATT TAATATGGACTAAAGGAGGCTTTT
F205	TCGTCGGCAGCGTC AGATGTGTATAAGAGACAG (N1:25252525)(N1)(N1) (N1)(N1)(N1) (N1)(N1)ATCACGT TAATATGGACTAAAGGAGGCTTTT
F206	TCGTCGGCAGCGTC AGATGTGTATAAGAGACAG (N1:25252525)(N1)(N1) (N1)(N1)(N1) (N1)(N1)CAGATCT TAATATGGACTAAAGGAGGCTTTT
F207	TCGTCGGCAGCGTC AGATGTGTATAAGAGACAG (N1:25252525)(N1)(N1) (N1)(N1)(N1) (N1)(N1)GGCTACT TAATATGGACTAAAGGAGGCTTTT
F208	TCGTCGGCAGCGTC AGATGTGTATAAGAGACAG (N1:25252525)(N1)(N1) (N1)(N1)(N1) (N1)(N1)TAGCTTT TAATATGGACTAAAGGAGGCTTTT
F209	TCGTCGGCAGCGTC AGATGTGTATAAGAGACAG (N1:25252525)(N1)(N1) (N1)(N1)(N1) (N1)(N1)TTAGGCT TAATATGGACTAAAGGAGGCTTTT
F210	TCGTCGGCAGCGTC AGATGTGTATAAGAGACAG (N1:25252525)(N1)(N1) (N1)(N1)(N1) (N1)(N1)ACTTGAT TAATATGGACTAAAGGAGGCTTTT
F211	TCGTCGGCAGCGTC AGATGTGTATAAGAGACAG (N1:25252525)(N1)(N1) (N1)(N1)(N1) (N1)(N1)GATCAGT TAATATGGACTAAAGGAGGCTTTT
F212	TCGTCGGCAGCGTC AGATGTGTATAAGAGACAG (N1:25252525)(N1)(N1) (N1)(N1)(N1) (N1)(N1)CTTGTAT TAATATGGACTAAAGGAGGCTTTT

Step 1 reverse primers:

R301	GTCTCGTGGGCTCGG AGATGTGTATAAGAGACAG (N1:25252525)(N1)(N1) (N1)(N1)(N1) (N1)(N1)TATATACGC TCGAATTCAAGCTTAGATCTGATA
R302	GTCTCGTGGGCTCGG AGATGTGTATAAGAGACAG (N1:25252525)(N1)(N1) (N1)(N1)(N1) (N1)(N1)CGCTCTATC TCGAATTCAAGCTTAGATCTGATA
R303	GTCTCGTGGGCTCGG AGATGTGTATAAGAGACAG (N1:25252525)(N1)(N1) (N1)(N1)(N1) (N1)(N1)GAGACGTCT TCGAATTCAAGCTTAGATCTGATA
R304	GTCTCGTGGGCTCGG AGATGTGTATAAGAGACAG (N1:25252525)(N1)(N1) (N1)(N1)(N1) (N1)(N1)ATACTGCGT TCGAATTCAAGCTTAGATCTGATA
R305	GTCTCGTGGGCTCGG AGATGTGTATAAGAGACAG (N1:25252525)(N1)(N1) (N1)(N1)(N1) (N1)(N1)ACTAGCAGA TCGAATTCAAGCTTAGATCTGATA
R306	GTCTCGTGGGCTCGG AGATGTGTATAAGAGACAG (N1:25252525)(N1)(N1) (N1)(N1)(N1) (N1)(N1)TGAGCTAGC TCGAATTCAAGCTTAGATCTGATA
R307	GTCTCGTGGGCTCGG AGATGTGTATAAGAGACAG (N1:25252525)(N1)(N1) (N1)(N1)(N1) (N1)(N1)CTGCTACTC TCGAATTCAAGCTTAGATCTGATA
R308	GTCTCGTGGGCTCGG AGATGTGTATAAGAGACAG (N1:25252525)(N1)(N1) (N1)(N1)(N1) (N1)(N1)GCGTACGCA TCGAATTCAAGCTTAGATCTGATA

For the first step for PCR, we performed 8 or 16 reactions per sample, using ~4.8ug (ranging between 3ug and 7.5ug) of DNA per sample across all reactions. Each set of eight 50 µL reactions included 16 µ of 50mM MgCl2, 8 µL of 10 µM forward primer, 8 µL of 10 µM reverse primer, template DNA, and 200 µL of OneTaq HotStart 2X Master mix (NEB #M0484L). Three cycles of PCR was then carried out with the following steps:

1. 94°C for 10min
2. 94°C for 3min
3. 55°C for 1min
4. 68°C for 1 min
5. Repeat steps 2-4 twice for a total of 3 cycles
6. 68°C for 1min
7. Hold at 4°C

The first-step PCR product was then column purified using the GeneJET Gel Extraction Kit (#K0692). Briefly, 100 µL of orange binding buffer were added to each 50 µL reaction. All 8 or 16 reactions from a given sample were pooled into the same purification column in a vacuum manifold. We then washed the column with 750 µL of wash buffer over vacuum. Then, each column was spun for 30s at max speed to remove residual wash buffer. We then eluted into 47 µL of nuclease free water by centrifuging and stored the samples at 4°C for the second step of PCR.

The second step of PCR further amplifies the barcodes and attaches Illumina indices as well as P5, P7 sequences for compatibility with Illumina sequencing, as done previously (Kinsler, Geiler-Samerotte, and Petrov 2020; Kinsler et al. 2023). We used Nextera Index Xt v2 primers (Illumina #FC-131–2004) with the following sequences:

S513	AATGATACGGCGACCACCGAGATCTACACTCGACTAGTCGTCGGCAGCGTC
S515	AATGATACGGCGACCACCGAGATCTACACTTCTAGCTTCGTCGGCAGCGTC
S516	AATGATACGGCGACCACCGAGATCTACACCCTAGAGTTCGTCGGCAGCGTC
S517	AATGATACGGCGACCACCGAGATCTACACGCGTAAGATCGTCGGCAGCGTC
S518	AATGATACGGCGACCACCGAGATCTACACCTATTAAGTCGTCGGCAGCGTC
S520	AATGATACGGCGACCACCGAGATCTACACAAGGCTATTCGTCGGCAGCGTC
S521	AATGATACGGCGACCACCGAGATCTACACGAGCCTTATCGTCGGCAGCGTC
S522	AATGATACGGCGACCACCGAGATCTACACTTATGCGATCGTCGGCAGCGTC
N716	CAAGCAGAAGACGGCATACGAGATTAGCGAGTGTCTCGTGGGCTCGG
N718	CAAGCAGAAGACGGCATACGAGATGTAGCTCCGTCTCGTGGGCTCGG
N719	CAAGCAGAAGACGGCATACGAGATTACTACGCGTCTCGTGGGCTCGG
N720	CAAGCAGAAGACGGCATACGAGATAGGCTCCGGTCTCGTGGGCTCGG
N721	CAAGCAGAAGACGGCATACGAGATGCAGCGTAGTCTCGTGGGCTCGG
N722	CAAGCAGAAGACGGCATACGAGATCTGCGCATGTCTCGTGGGCTCGG
N723	CAAGCAGAAGACGGCATACGAGATGAGCGCTAGTCTCGTGGGCTCGG
N724	CAAGCAGAAGACGGCATACGAGATCGCTCAGTGTCTCGTGGGCTCGG
N726	CAAGCAGAAGACGGCATACGAGATGTCTTAGGGTCTCGTGGGCTCGG
N727	CAAGCAGAAGACGGCATACGAGATACTGATCGGTCTCGTGGGCTCGG
N728	CAAGCAGAAGACGGCATACGAGATTAGCTGCAGTCTCGTGGGCTCGG
N729	CAAGCAGAAGACGGCATACGAGATGACGTCGAGTCTCGTGGGCTCGG

Note that because of increased risk of index swapping associated with sequencing amplicons on Illumina machines with ExAmp technology (Kinsler et al. 2023), we labeled each sample with a unique combination of inline and Illumina indices. This allows for reads associated with index swapping due to mis-incorporation of indices or template swapping on the sequencing machine to be identified and removed from downstream analysis.

For the second step of PCR, we performed 3 reactions per sample. For each set of thee 50 µL reactions, we used 45 µL of column purified Step 1 PCR product, 2.5 µL of the designated forward Nextera XT Index V2 primer (e.g., N716), 2.5 µL of the designated reverse Nextera XT Index V2 primer (e.g., S513), 3 µL of 10mM dNTP (Fisher Scientific #PR-U1515), 1.5 µL of Q5 polymerase (NEB #M0491L), 30 µL of Q5 buffer (NEB #M0491L), and 65.5 µL of nuclease free water. We then ran the following program on the thermocycler to amplify for 20 cycles:

1. 98°C 30s
2. 98°C 10s
3. 62°C 20s
4. 72°C 30s
5. Repeat steps 2-4 19 times (20 cycles total)
6. 72°C 3min
7. Hold at 4 C

We then performed column purification following a similar procedure to the purification from step 1, eluting instead into 30 µL of nuclease free water.

Following the second step of PCR, in order to further remove any residual ancestral barcode that were not digested before PCR amplification, we performed a second round of ApaLI digestion, adding 3.5 µL of Cutsmart buffer and 1 µL of ApaLI restriction enzyme (NEB

#R0507L) to each sample's Step 2 PCR product, digesting for at least 1 hr at 37°C. We then performed gel extraction using the GeneJet gel purification kit for each sample, keeping the 350bp band representing intact barcode sequences. We then quantified the DNA concentration for each sample using Qubit HS kit (ThermoFisher #Q32854), pooled such that each sample was equally represented in the final library, and submitted for sequencing on Illumina sequencing machines.

Tracking evolution

To track the dynamics of the evolution experiment, estimate the fitness of lineages during the evolution experiment, and infer the distribution of fitness effects, we extracted DNA and used PCR amplification to generate libraries for sequencing as described above, with the exception of not performing the ApaLI restriction digestion.

In order to identify barcode counts over time, we followed previously used custom scripts along with bartender (https://github.com/Sherlock-Lab/Barcode_seq/blob/master/bartender_BC1_BC2.py) to extract and cluster barcodes from timepoints along the evolution trajectory.

To infer fitness effects, the mean fitness of the population, and infer the from the evolution experiments themselves, we used FitMut1 (Levy et al. 2015; F. Li, Mahadevan, and Sherlock 2023). To infer the distribution of fitness effects from this data, we used an approach developed in Levy et al 2015. The general idea of this approach is to infer the distribution of fitness effects by counting the number of mutants arising with selection coefficients in the interval [s, s+ds] across the course of the evolution experiment. To infer a rate, we adjust the amount of time that this mutant could have arisen and been detected based on the mean fitness of the population, the time it takes for the mutant to establish, and its ability to rise to a detectable frequency in the population. Specifically, the number of mutations in the interval [s, s+ds] is expected to be:

$$\text{number of mutations in } ds \;=\; \mu(s)ds \;\times\; (s/c) \;\times\; N_e \int_0^{t-(1/s)ln(n_0 s/c)} e^{-\bar{x}(t)}dt$$

Where N_e = 7x10^7 is the effective population size, $\bar{x}(t)$ is the mean fitness of the population over time, $c{\sim}3.5$ is the offspring number variance, and $n_0{\sim}1000$ is the effective lineage size. We invert this function to estimate $\mu(s)$.

Counting barcodes and calculating fitness from fitness measurement sequencing data

We used BarcodeCounter2 (Venkataram et al. 2016; *BarcodeCounter2: Count DNA Barcodes Version 2*, n.d.) to assign reads to their associated samples and barcodes. Briefly, we extracted the inline index, barcode, and UMI regions from each read using BLAST (Altschul et al. 1990) to the known constraint region in the amplicon sequence. Then, we associated each read to its corresponding condition and timepoint based on its combination of Illumina and inline indices. We then used Bowtie2 (Langmead and Salzberg 2012) to map the extracted barcode regions to

our known list of barcodes in the experiment, used UMIs to avoid over-counting duplicate reads, and counted the number of barcodes per sample.

To infer fitness values, we used the fitness inference procedure as developed previously. In each time interval, a mutant's fitness is calculated as it's log-frequency change, adjusted by the mean fitness of the population. We infer the mean fitness of the population by calculating the log-frequency change of the set of 60 neutral lineages from Venkataram 2016.

Frequency dependence

During the analysis of the fitness measurement data, we noticed a systematic shift of fitness over the course of the experiment, with many barcoded mutants showing a decline in fitness fitness in 1- and 2-Day experiments as the fraction of the population that was adaptive increased, even after adjustment for changes in mean fitness (Figure S1). These trends were not identified in previous experiments, and we suspect that this is due to frequency-dependent fitness effects driven by the very strongly adaptive mutants. To avoid the influence of these effects, we used only the first timepoint interval from 2-Day experiments (from timepoint 0 to timepoint 1), as this kept our fitness measurements consistent with previous studies [cite Kinsler, Li]. Throughout the rest of the study, 2-Day fitness refers to this measurement using only early timepoints.

Quantifying performances

To quantify mutant performances in each phase of growth, we quantified differences between fitnesses inferred from 1-, 2-, 3-, and 5-Day transfer experiments. Because the time interval between 24 and 48 hours only contains respiration phase, we quantified respiration performance per hour as:

ResPerHour = 2-Day fitness - 1-Day fitness / 24hrs

To calculate fermentation performance, we removed the 4 hours worth of respiration performance from the 1-Day fitness and divided the remaining fitness into the 16 hours of fermentation performance (accounting for ~4 hours of lag phase):

FerPerHour = (1-Day fitness - 4*ResPerHour) / 16hrs

Because 1-Day fitness measurements are used for both respiration and fermentation performances, there is the potential for noise in 1-Day measurements to introduce a relationship between fermentation and respiration performances. To eliminate measurement noise from having this influence, we used different replicates of the 1-Day fitness to calculate fermentation and respiration performance. Specifically, we used the replicate 2 flasks to calculate respiration performance and the replicate 1 flasks to calculate fermentation performance.

To infer stationary phase performance, we took the difference between 5- and 3-day fitness and divided by 48hrs of time:
StaPerHour = (5-Day fitness - 3-Day fitness) / 48hrs

To calculate the uncertainty of performances, we used error propagation from the estimated errors of fitness. To calculate performances relative to parental strain, we computed the difference between each mutant's performance and its parental strain. For *CYR1, GPB2, TOR1,* and *IRA1-missense* second-step mutations, we used the mean of the neutral barcode strains as the parental reference measurement. For *IRA1-nonsense* second-step mutations, for which no neutral clones were isolated, we used the parental barcoded barcoded mutant present in the pool of first-step mutants (denoted with a "+" in main text figures).

Differences in selection pressure do not drive the shift towards modular adaptation

To evaluate whether a systematic shift in selection pressure occurred during the second-step evolution experiments, we identified mutants for which we called their evolution fitness from the estimation of the distribution of fitness effects. Because many of the remaining mutants are pure diploids whose spread may be dominated by measurement noise, we removed these mutants from the list. This resulted in a set of 185 second-step mutants. We then performed a partial correlation analysis between respiration performance and evolution fitness, accounting for fitness measurement fitness. We find no evidence of such a relationship ($p=0.74$, $r=-0.02$). Similarly, we find no relationship between fermentation performance and evolution fitness after accounting for fitness measurement fitness ($r=0.38$, $p=0.613$).

1-Day evolution experiment analysis

To evaluate whether yeast adapting to a 1-Day transfer could further improve their fermentation performance, we quantified the performance of 1-Day mutants as above. We identified several mutants with fermentation performances meeting or exceeding the maximum fermentation performance achieved by first-step mutants. Using a threshold of at least 2 standard errors (which corresponds to a FDR of $p<0.05$) a single second-step mutant that arose in the Evo1D *IRA1*-nonsense population had fermentation performance that exceeded the first-step maximum.

Whole genome sequencing

We selected mutants for whole genome sequencing based on their fitness and performance in the growth phase, such that we selected as many unique mutants as possible based on their performances and those that had barcodes confidently identified by the metagrid. This resulted in a total of 346 clones targeted for sequencing.

Clones that were selected for sequencing were grown in 500 µL of YPD in 96-well deep well plates for 2 days at 30°C without shaking. 400 µL of saturated culture was collected from each

well for genomic DNA extraction using the Invitrogen PureLink Pro 96 Genomic DNA Kit. Libraries were prepared using a ⅕ dilution protocol of the Illumina DNA prep, using Illumina Unique Dual Indexing primers.

Variant calling

To identify variants from the sequencing data, we used bwa (H. Li and Durbin 2009) to align all reads to the S288C reference genome (R64-1-1-20110203). We then used picard (https://broadinstitute.github.io/picard/) to fix read groups and marked duplicate reads. We then used GATK (version 4.2.0.0) (Van der Auwera and O'Connor 2020) to generate individual GVCF files, merge GVCF files, and call genotypes on all samples. After removing samples with less than 20x coverage, we removed variants according to the following filters: QD < 5, FS < 60, SOR < 3, M! < 50, MQRankSum < -3.0, ReadPosRankSum < -5.0. After this filtering, we further removed ancestral variants present in all samples, mitochondrial variants, variants with GQ less than 70. This filtering resulted in 727 sites that were variable across our samples. We then manually inspected all called variants, resulting in 631 manually verified variants. We then used bcftools (H. Li 2011) to filter the vcf file to these verified variants and used snpEff (Cingolani et al. 2012) to annotate variants.

We then assigned variants to the corresponding barcoded mutants based on plate position. To check that our assignment was correct, we also verified the barcodes from the whole genome sequencing reads. For the 326 mutants for which we had sufficient coverage of the barcode region (at least 4 successfully-mapped barcode reads), 324 had the correct barcode identified. We opted to not use sequencing information from the 2 samples with mismatching barcodes between the sequencing and expected based on clone isolation barcode sequencing.

We further identified pre-existing mutations in which identical mutations were present in several sequenced mutants of a given low-complexity barcode. These mutations were classified as "pre-existing" mutations and ignored in downstream analyses except in cases where they belonged to a putatively causal gene (see "Mutation and ploidy classification" section).

Mutation and ploidy classification

To identify mutations likely responsible for driving fitness gains in these experiments, we identified putative adaptation-driving mutations by identifying mutations that occurred in genes that were recurrently mutated across adaptive clones. Specifically, genes with 4 or more mutations were classified as likely adaptation-driving. After classifying genes based on their function, we further identified additional mutations as adaptation-driving due to their effect on similar processes as recurrently mutated genes.

To classify the ploidy of mutations, we initially classified mutants according to their performance in the benomyl assay. We additionally classified mutants as "pure diploids" and "neutral haploids" by their similarity to the large cluster of haploids and diploids in terms of their fitness

effects across all the conditions. Mutants that were within this large cluster of diploids but initially classified as haploids according to the benomyl assay were classified as pure-diploids.

From this initial ploidy classification, the majority of mutants which exhibited mutations in *PAB1* were classified as diploids, perhaps reflecting a sensitivity of *PAB1* mutants to benomyl. We re-classified all *PAB1* mutants as adaptive haploids with respiration performance relative to parental strain less than 0.06. *PAB1* mutants with greater respiration performance were classified as high-fitness diploids, consistent with the effect that auto-diploidization had on mutations from other genes. Similarly, *PAN2* and *PAN3* mutants were classified as diploids and have previously been shown to be susceptible to benomyl (Brown et al. 2006). Given we had few of these mutations, we did not have enough information to reclassify these mutations as we did for *PAB1.*

Data availability

Raw sequencing data is available on Short Read Archive under BioProject Number: PRJNA1098711. Processed frequency counts, fitness data, performance data, and mutational calls are available on Github: https://github.com/grantkinsler/EvolvingFront. All yeast strains are available upon request.

Code availability

Code for all data processing and figure generation is available on Github: https://github.com/grantkinsler/EvolvingFront

SUPPLEMENTARY FIGURES

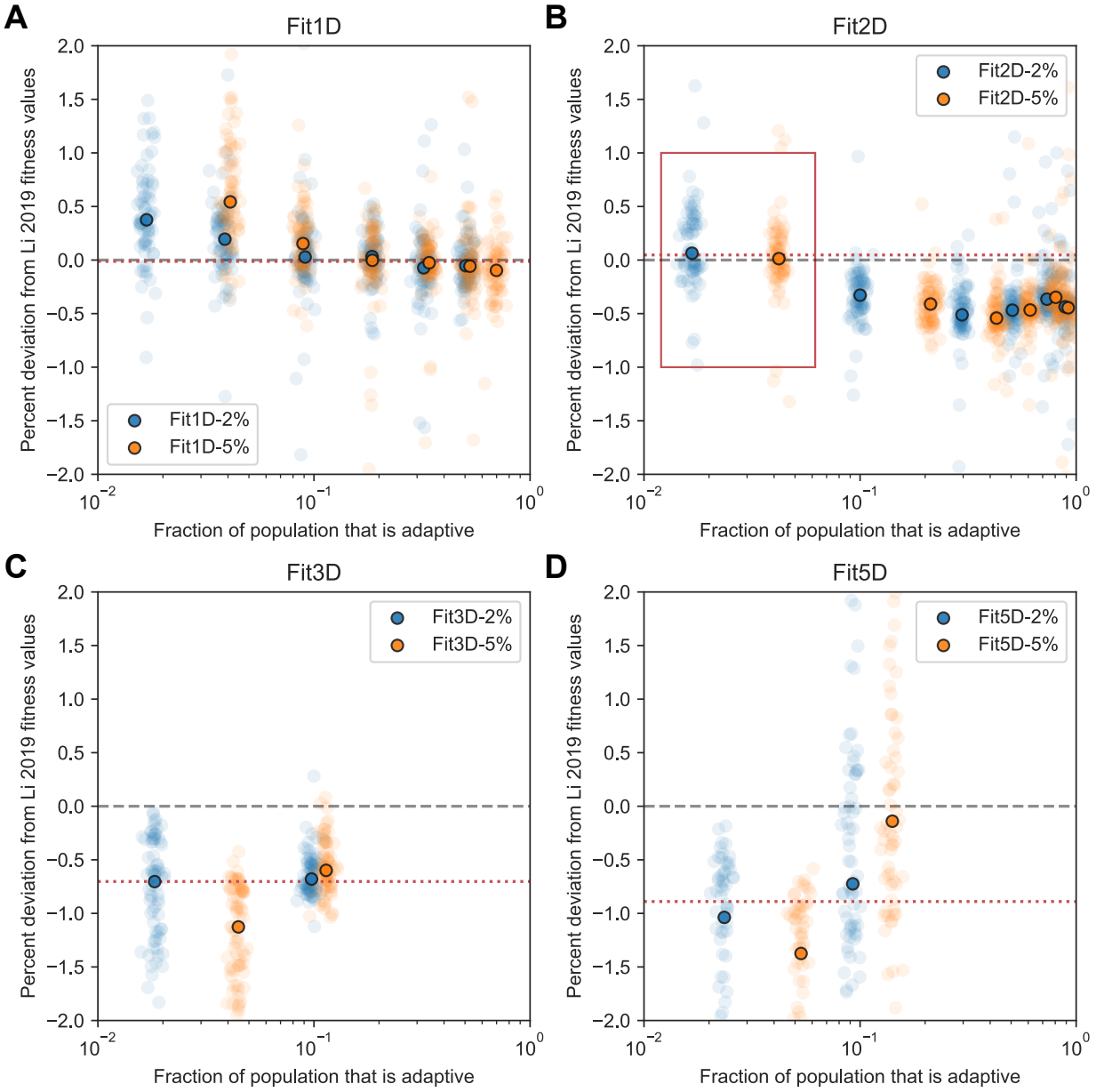

Fig S1. Evidence for frequency dependence in fitness measurement experiments. The vertical axis of each subplot depicts the percent deviation from Li 2019 fitness values for the set of adaptive haploids that were present in Li 2019 fitness measurements and this study. The horizontal axis is the fraction of the population that is adaptive. Points show the deviation for each mutant, with the median across all mutants depicted by the heavy circle. Blue and orange points are from experiments initiated with the adaptive barcode pool consisting of 2% and 5% of the population, respectively. Red dotted line indicates the deviation for the overall fitness measurement used throughout the paper. Red box in (B) refers to the timepoints used. Subpanels A-D refer to Fit1D, Fit2D, Fit3D, and Fit5D fitness values, respectively.

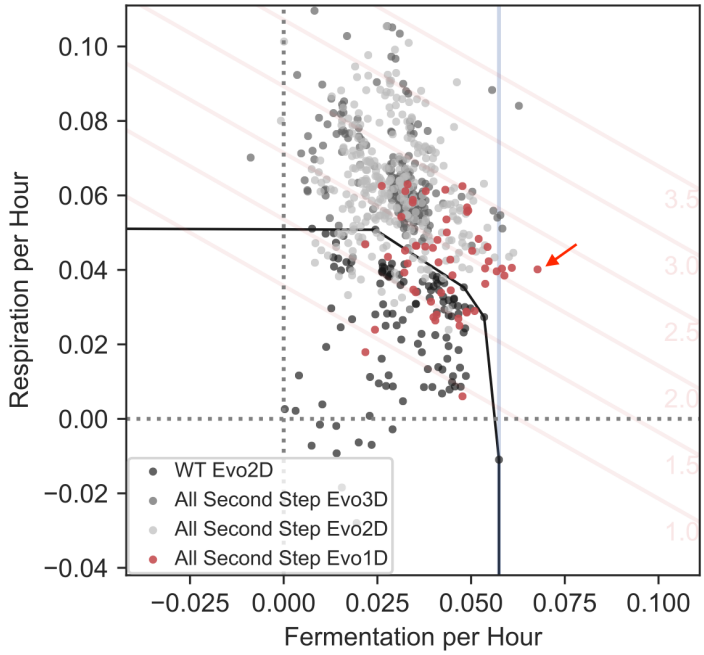

Fig S2. 1-Day evolution experiments identify mutants that improve fermentation performance. Fermentation and respiration performances for mutants discussed in the main text and Evo1D mutants (in red). Despite less dense sampling, we find at least one Evo1D mutant (indicated with red arrow) with fermentation performance that exceeds the highest fermentation performance from first-step mutants (blue vertical line).

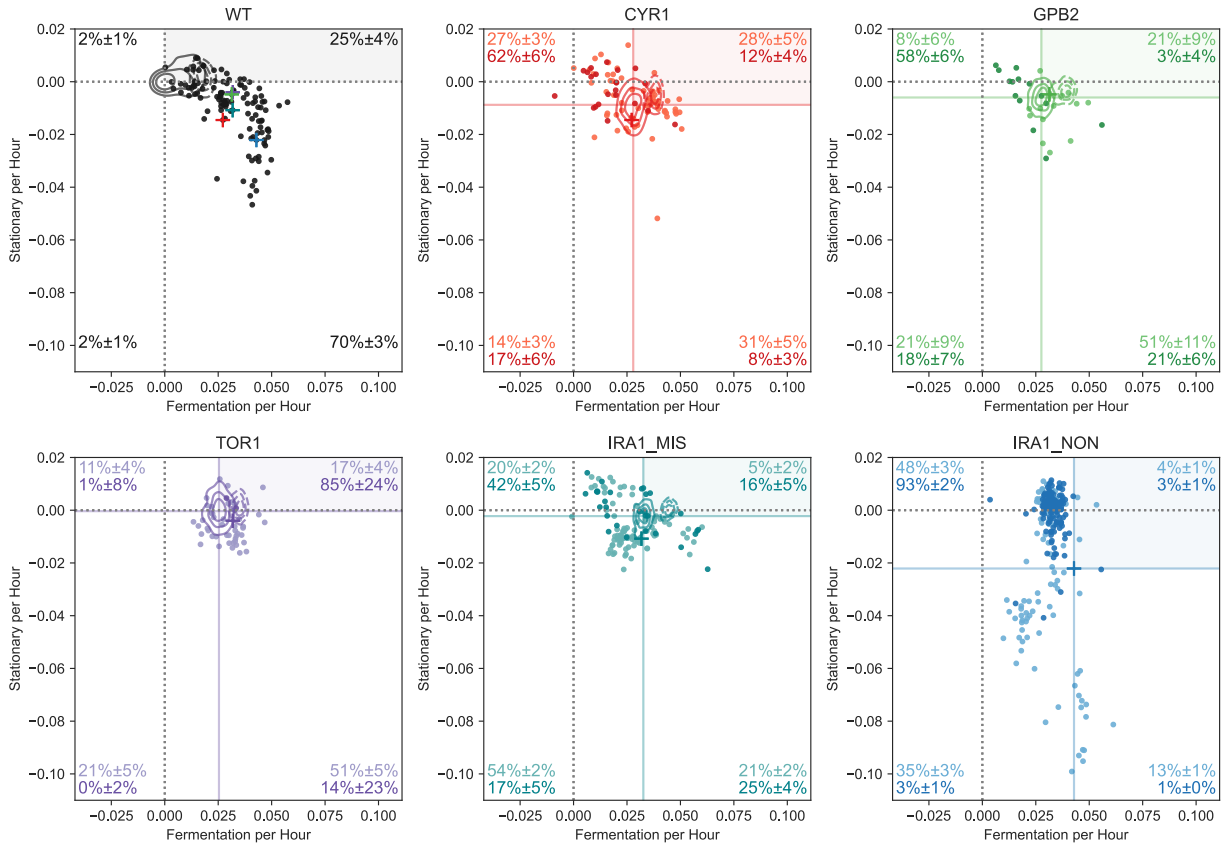

Fig S3. **Fermentation and stationary phase performances by parental strain.** Each subpanel depicts a scatter plot with the fermentation and stationary performances for each parental strain. Lighter points indicate Evo2D mutants, darker points indicate Evo3D mutants.

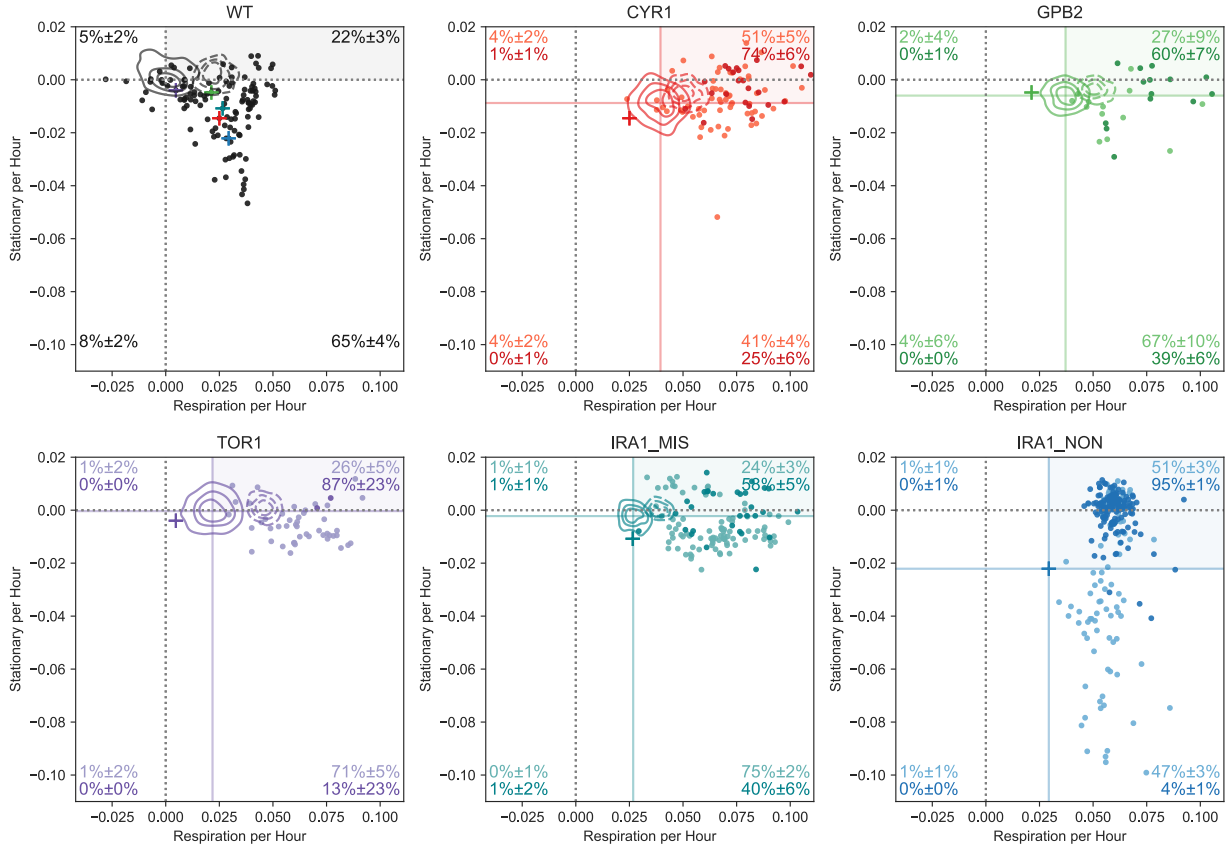

Fig S4. Respiration and stationary phase performances by parental strain. Each subpanel depicts a scatter plot with the respiration and stationary performances for each parental strain. Lighter points indicate Evo2D mutants, darker points indicate Evo3D mutants.

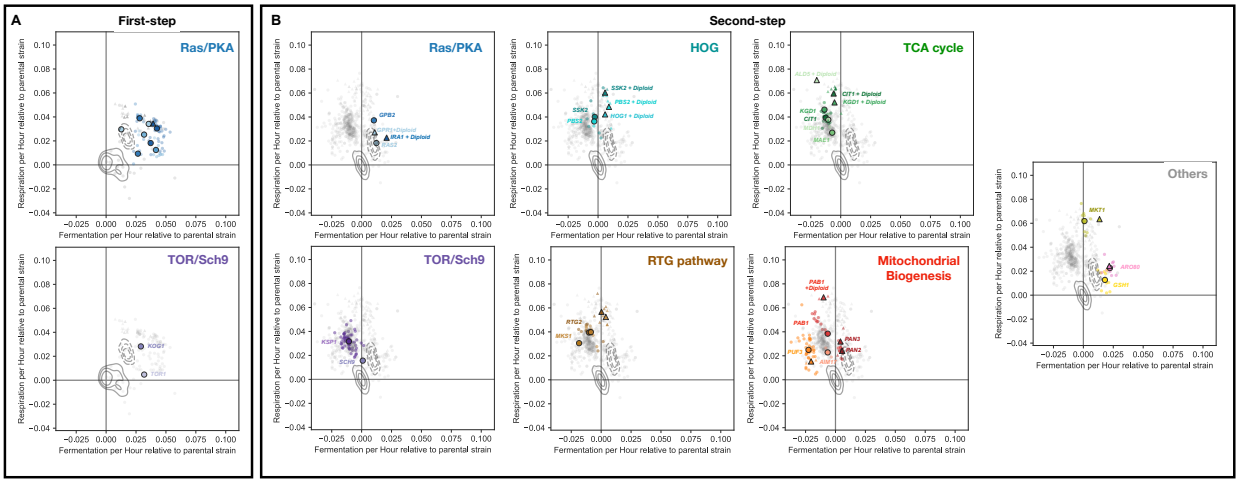

Fig S5. Molecular targets of adaptation by gene. Performance effects of mutations separated by biological process or pathway as in Table 1. Points are colored by gene, and shape indicates ploidy (circles are haploids, triangles diploids). KDE estimates show density of neutral haploids for each parental strain (solid lines) and pure diploids for each parental strain (dashed lines). **(A)** First-step mutants. **(B)** Second-step mutants depicted, with performances measured relative to parental strain.

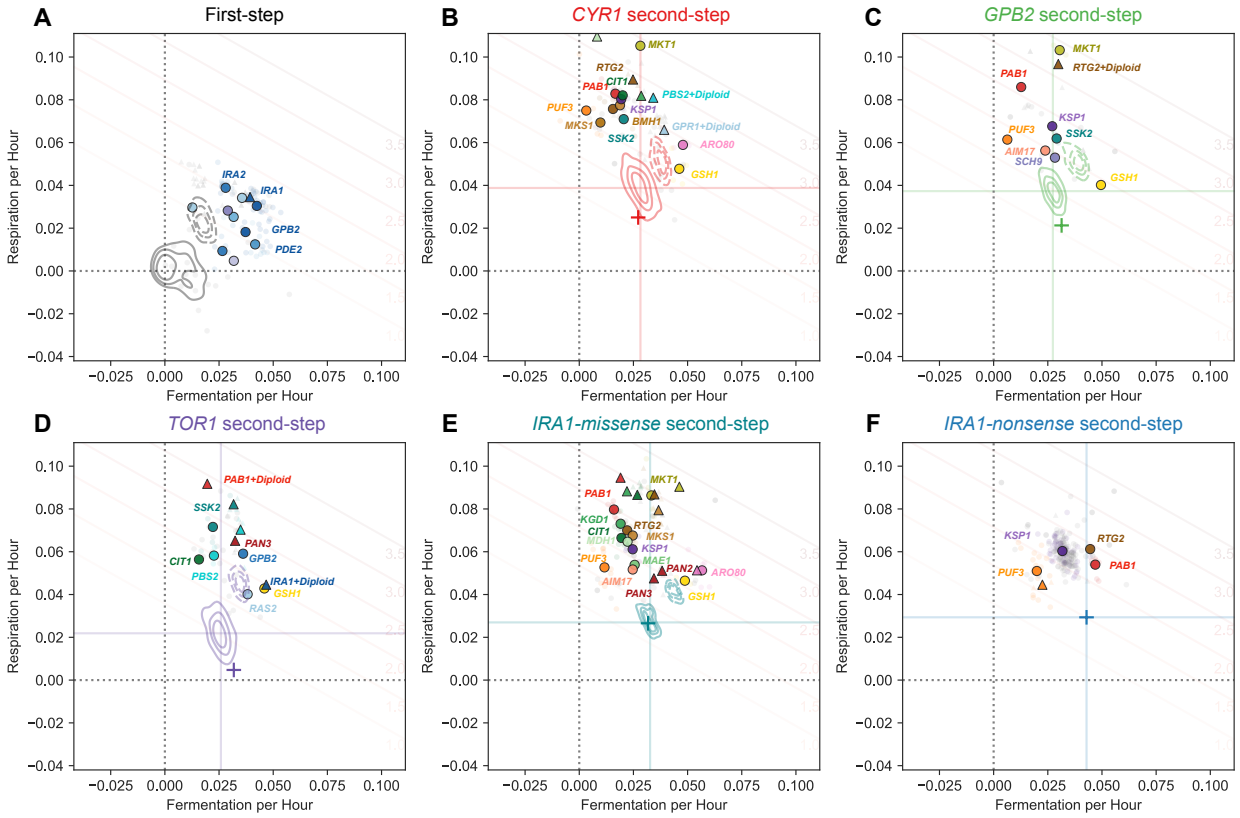

Fig S6. Molecular targets of adaptation by gene. Colored by gene, shape depicts ploidy (circles are haploids, triangles diploids). KDE estimates show density of neutral haploids for each parental strain (solid lines) and pure diploids for each parental strain (dashed lines).

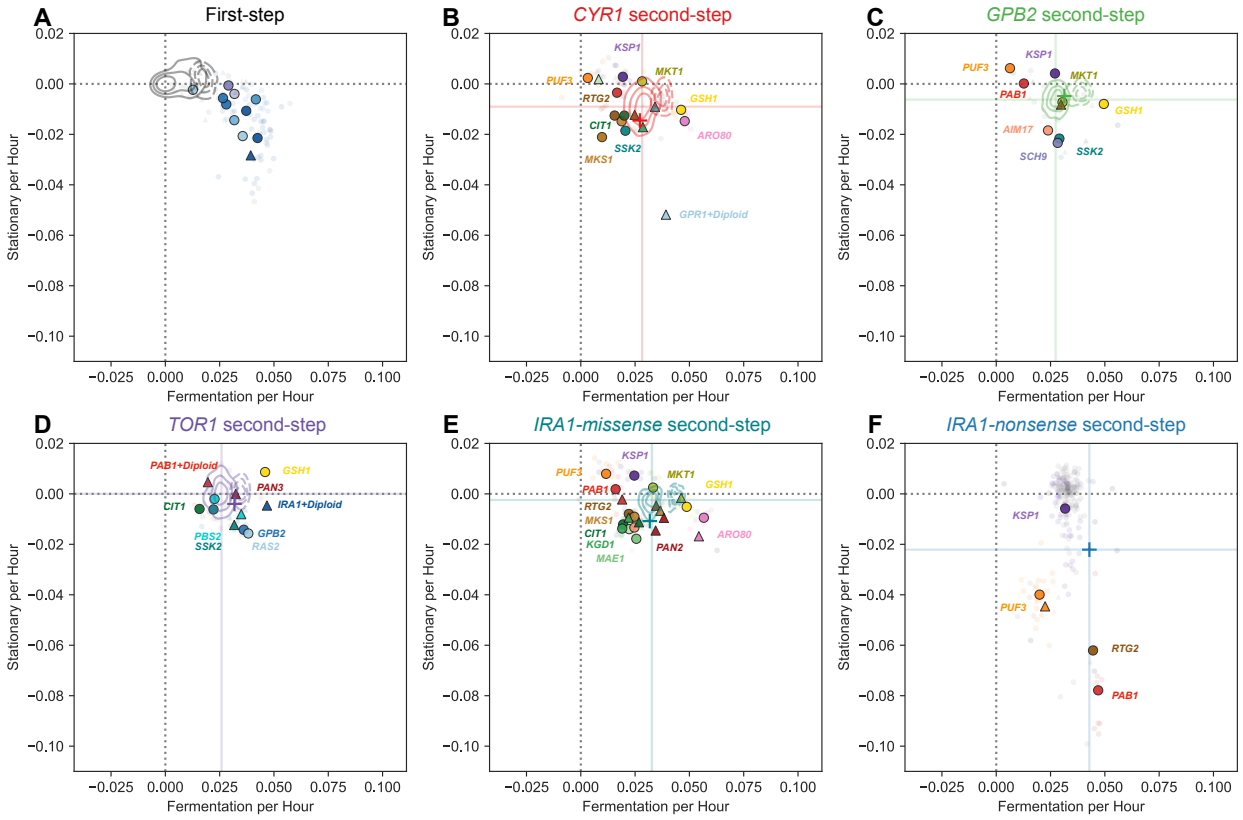

Fig S7. Mutational effects on fermentation and stationary phase performance. Colored by gene, shape depicts ploidy (circles are haploids, triangles diploids). KDE estimates show density of neutral haploids for each parental strain (solid lines) and pure diploids for each parental strain (dashed lines).

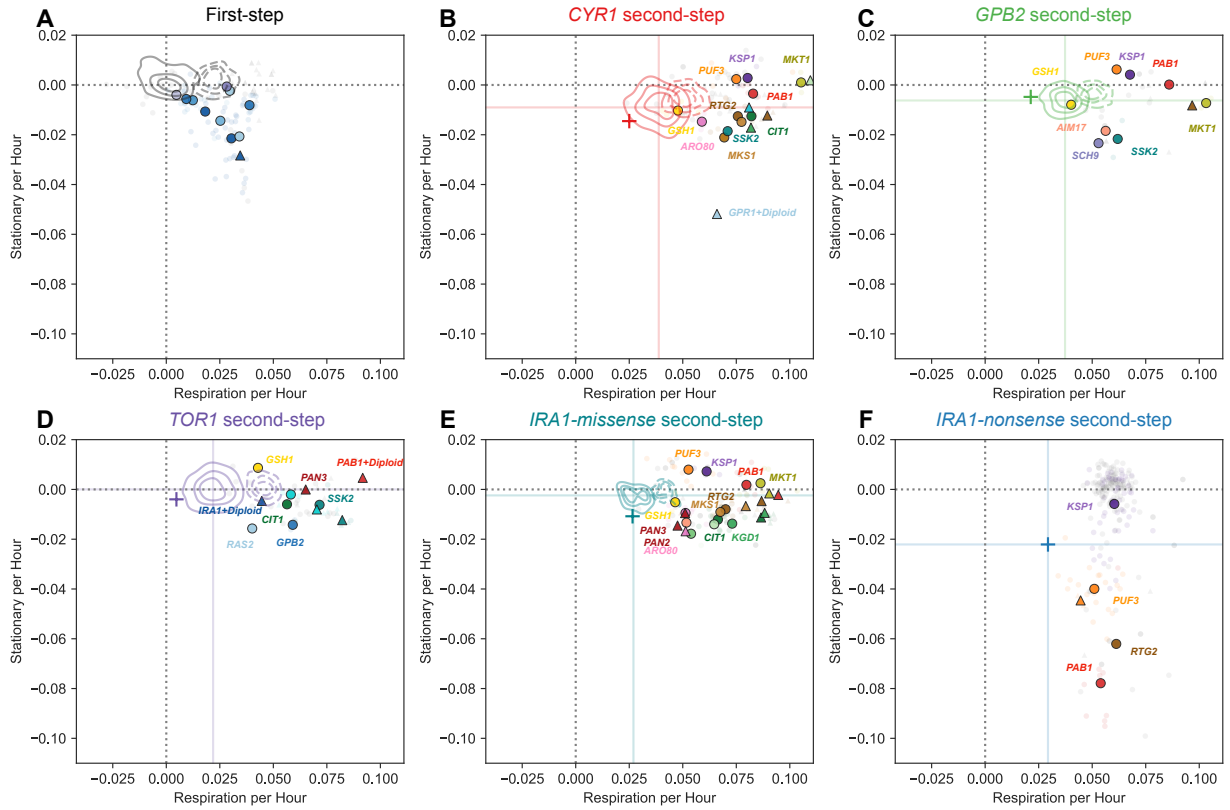

Fig S8. Mutational effects on respiration and stationary phase performance. Colored by gene, shape depicts ploidy (circles are haploids, triangles diploids). KDE estimates show density of neutral haploids for each parental strain (solid lines) and pure diploids for each parental strain (dashed lines).